

OPEN ACCESS

EDITED BY

Marianna Tosato,

Simon Fraser University, Canada

REVIEWED BY
Susovan Jana,
National Institute of Mental Health (NIH),
United States
Asti Mattia,
IRCCS Local Health Authority of Reggio

*CORRESPONDENCE Ivis F. Chaple ⋈ ichaple@utk.edu

Emilia, Italy

RECEIVED 30 June 2025
ACCEPTED 26 August 2025
PUBLISHED 11 September 2025

CITATION

Racz DG and Chaple IF (2025) Platinum group metals for nuclear medicine, a luxurious dream or the future of imaging and therapy: a review.

Front. Nucl. Med. 5:1656374. doi: 10.3389/fnume.2025.1656374

COPYRIGHT

© 2025 Racz and Chaple. This is an openaccess article distributed under the terms of the Creative Commons Attribution License (CC BY). The use, distribution or reproduction in other forums is permitted, provided the original author(s) and the copyright owner(s) are credited and that the original publication in this journal is cited, in accordance with accepted academic practice. No use, distribution or reproduction is permitted which does not comply with these terms.

Platinum group metals for nuclear medicine, a luxurious dream or the future of imaging and therapy: a review

Daniel G. Racz and Ivis F. Chaple*

Department of Nuclear Engineering, University of Tennessee, Knoxville, TN, United States

Platinum group metals (PGMs) consist of six transition metals: platinum (Pt), palladium (Pd), rhodium (Rh), osmium (Os), iridium (Ir), and ruthenium (Ru). PGMs have been used notably in industrial, electronic, and medical applications. For example, Ir-192 is often utilized in industry to detect structural defects in metal and assess pipeline integrity. Pd-104 is irradiated to produce Pd-103 seeds, used for prostate cancer treatment. Other isotopes of elements in this group can be sourced to facilitate critical applications, discussed in this review. Due to their unique chemical and nuclear properties, these metals may be promising candidates for various nuclear medicine applications, including diagnostic imaging via Positron Emission Tomography (PET), Single Photon Emission Computed Tomography (SPECT) and Targeted Radionuclide Therapy (TRT). This review will explore PGMs in nuclear medicine, focusing on their production routes, nuclear characteristics, and suitability for past and future development of radiopharmaceuticals. We will highlight methods for radiochemical separation and purification of each radionuclide, discussing potential challenges and emphasizing the need for further research to ensure sustainability. As the demand for advanced nuclear medicine techniques continues to grow, PGMs may play a significant role in addressing current challenges in the field. We will discuss several radionuclides of interest to nuclear medicine including ¹⁹¹Pt, ^{193m}Pt, ^{195m}Pt, ¹⁰³Pd, ¹⁰⁹Pd, ^{103m}Rh, ¹⁰⁵Rh, ¹⁹¹Os, ¹⁹²Ir, ⁹⁷Ru, and ¹⁰³Ru.

KEYWORDS

platinum group metals, platinum, palladium, rhodium, osmium, iridium, ruthenium, nuclear medicine

1 Introduction

Cancer remains one of the leading global health concerns, with an estimated 19.3 million new cancer cases and 10 million cancer-related deaths worldwide in 2020 (1), and projections are expected to rise by 60% within the next two decades (2). The increase incidence of cancer necessitates the development of innovative approaches towards both cancer diagnosis and treatment. Nuclear medicine provides powerful tools for both diagnostic imaging and therapy. Techniques such as position emission tomography (PET) and single photon emission computed tomography (SPECT) offer functional imaging capabilities that are crucial for accurately detecting cancerous cells. By administering a radiopharmaceutical that targets cancer-specific cells, nuclear medicine imaging can detect the radiation emitted from the radiopharmaceuticals, enabling personalized treatment planning. Therefore, these imaging modalities are

crucial in clinical practice, guiding oncologists in selecting optimal conditions to improve patient outcomes. Beyond diagnostics, targeted radionuclide therapy (TRT) has been utilized as a cornerstone in oncology care. Radionuclides have also played vital roles alongside external beam radiation therapy (EBRT). For example, ¹⁹²Ir sources are widely used in high dose rate brachytherapy for many types of cancers (3), and ¹⁰⁶Ru is used as a standard eye-preserving treatment for uveal melanoma (4). Whether a radionuclide is used in either diagnostic imaging or radiotherapeutics, the continued exploration of their application is of key importance towards nuclear medicine advancement.

The discovery of the six platinum group metals (PGMs) platinum (Pt), palladium (Pd), rhodium (Rh), osmium (Os), iridium (Ir), and ruthenium (Ru)-spanning from the sixteenth to the nineteenth centuries, laid the foundation for advancements across diverse fields. Platinum was first discovered in the sixteenth century in Colombia's Choco district, where four additional PGMs-palladium, rhodium, osmium, and iridiumwere classified three centuries later by William H. Wollaston and Smithson Tenant (5). Wollaston discovered palladium and rhodium by refining platinum ores, where Tennant discovered iridium and osmium in the residues (5). The sixth PGM, ruthenium, was extracted by Karl Klaus in 1844 from platinum residues, and named after "Ruthenia" (Latin for Russia) (5, 6). Today, these elements are integral not only in everyday technologies such as electronics and automotive catalysts but also in innovative medical treatments, where their unique propertieschemical, physical, nuclear—enable breakthroughs in cancer therapies, imaging, and radiopharmaceuticals.

Platinum-based compounds, especially in the oxidation states of 2+ and 4+, have been widely, and successfully, utilized for the treatment of many types of cancers (2, 7). The two most notable platinum-based chemotherapy agents are cisplatin and carboplatin, although there are several other variations of these drugs which are mainly characterized by a central Pt atom surrounded by atoms of Cl, NH2, CH3, and others. The toxicity of these compounds has become a major limitation in their use, as it can to some extent, have a negative effect on all organs (8). New strategies, such as the development of Pt(IV) prodrugs have been described to overcome the effects that diminish clinical outcomes (7). Palladium has shown similarities between the coordination chemistry of Pd(II) and Pt(II) compounds, advocating studies to implement Pd(II) complexes as antitumor drugs (9-11). Furthermore, described in Lazarevic et al. (11), Pd (II) compounds exchange ligands 10⁴-10⁵ times faster than corresponding Pt(II) analogs—with various compounds showing anti-inflammatory, antimicrobial (12), antitumor (13), antibacterial, antiviral, and antifungal capabilities (14). Ma et al. (15) stated that research into bioactive rhodium complexes are warranted and may eventually lead to the discovery of drugs with distinct mechanisms of action compared to traditional platinum or ruthenium-based therapeutics. Due to the wellknown toxicity of OsO4, osmium's utility in medicinal chemistry has been less explored; however, the implementation of novel ligands and the diverse coordination geometries and oxidation states of this metal has led to further development (16)—with several papers discussing potential osmium anticancer agents (17, 18). Konkankit et al. (16) highlighted a surge in the application of iridium complexes as anticancer agents and imaging probes, for example, octahedral cyclometalated iridium complexes, along with complexes targeting DNA and inhibiting specific proteins. Ruthenium has emerged as a "next-generation" therapeutic metal, while offering several advantages over Pt-based drugs, including electronic structure, tunable redox properties, and a relatively low toxicity profile contributing to its increasing importance (2, 7).

In addition to PGM compounds being utilized in traditional medicine, PGMs also contribute towards nuclear medicine due to useful nuclear decay properties essential for imaging or radionuclide therapy. In this review, a detailed evaluation of select PGM radionuclides, tracing their past developments and current successes or challenges towards advancement in nuclear medicine. Their nuclear properties will also be discussed, along with reviewing production routes and radiochemical separation methods that enable high purity radionuclide preparation. Moreover, key results from either pre-clinical or clinical studies, are reported, along with a discussion on how PGMs may be added as novel tools to the toolkit of modern nuclear medicine. Through this review, we aim to illustrate whether PGMs are a luxurious dream or a key to the future of molecular imaging and radionuclide therapy.

2 Platinum and platinum-based radionuclides

Naturally occurring platinum isotopes include: 190 Pt (0.012%,), 192 Pt (0.782%), 194 Pt (32.864%), 195 Pt (33.77%), 196 Pt (25.21%), and 198 Pt (7.356%) (19). For this review, we will focus on 191 Pt, $^{193\text{m}}$ Pt, and $^{195\text{m}}$ Pt, as other radioisotopes (188 Pt, 189 Pt, 197 Pt) have not been widely studied.

2.1 Platinum-191, ¹⁹¹Pt

Due to its nuclear decay properties, ¹⁹¹Pt may be suitable for Auger electron therapy. This radionuclide has a half-life of 2.83 d and decays 100% by electron capture (EC), with notable γ -ray energies of 538.9 keV (I_{γ} = 13.7%) and 465.5 keV (I_{γ} = 3.5%) (20).

2.1.1 Production and radiochemical separation of ¹⁹¹Pt

Multiple production routes for 191 Pt have been explored using either osmium or iridium targets bombarded with protons, deuterons, or α -particles highlighted in Table 1. Bonardi et al. (21) produced no-carrier-added (n.c.a.) 191 Pt—which complemented earlier work from Parent et al. (22) and Sharma and Smith (23)—while achieving 170 MBq/µg with decontamination factors of >10 6 via two optimized radiochemical separations (Sn(II)/ether vs. NH₂OH/dithizone extraction). Obata et al. (20) measured excitation functions, finding peak cross sections of ~623–635 mb for 191 Pt at ~26–

TABLE 1 Production pathways for platinum-based radionuclides.

Radionuclide	Nuclear reaction	Flux/Energy	References
¹⁹¹ Pt	natOs(α,xn) ¹⁹¹ Pt	$E_{\text{max}} = 38 \text{ MeV}$	(21, 260)
	¹⁹² Os(³ He,4n) ¹⁹¹ Pt	36 → 25 MeV	(261)
	natIr(p,xn)191Pt	E _{max} = 30 MeV	(20-22, 24, 262)
	natIr(d,xn)191Pt	$E_{\text{max}} = 40.3 \text{ MeV}$	(20, 260, 263)
^{193m} Pt	¹⁹² Os(α,3n) ^{193m} Pt	E _{max} = 39 MeV	(44, 45, 51)
	¹⁹² Pt(n,γ) ^{193m} Pt	4×10 ¹⁴ n cm ⁻² s ⁻¹	(52)
^{195m} Pt	193 Ir(n, γ) 194 Ir(n, γ) 195m Ir \rightarrow 195m Pt	$1-2.5 \times 10^{15} \text{ n}$ $\text{cm}^{-2} \text{ s}^{-1}$	(57, 59)
	¹⁹⁴ Pt(n,γ) ^{195m} Pt	$3-8.5 \times 10^{13} \text{ n}$ $\text{cm}^{-2} \text{ s}^{-1}$	(26, 59, 63, 64, 66)
	¹⁹⁵ Pt(n,n') ^{195m} Pt		(60)
	¹⁹² Os(α,n) ^{195m} Pt	28 → 16 MeV	(45)
	197 Au(γ ,n) 195m Pt	E _{max} = 34 MeV	(67)

32 MeV, with theoretical thick-target yields of ~108–192 MBq/ μ A-h for both proton and deuteron irradiation using ^{nat}Ir or ¹⁹³Ir targets. Furthermore, they noted ~25 MeV protons as the optimal energy, though advanced target dissolution methods were needed due to iridium exhibiting superior resistance to acid (20). Obata et al. (24) addressed this by using an alkalifused Ir target and *in situ* HCl digestion, followed by solvent extraction and anion exchange, yielding 17.4 ± 1.1 MBq/ μ A-h at EOB (7.1 ± 0.4 MBq/ μ A-h post separation) with >99% radionuclidic purity.

2.1.2 Applications of ¹⁹¹Pt

Areberg et al. (25) demonstrated the first use of [191Pt] cisplatin (Figure 1A) for tumor imaging. Fourteen patients received [191Pt] cisplatin (≥99% radionuclidic purity)—synthesis based on the work reported by Hoeschele et al. (26)—and showed clear gamma-camera visualization of tumors in multiple anatomical sites (25). Building on this, the same group (27) reported organ-specific absorbed and effective doses for [191Pt] cisplatin (and 193mPt/195mPt analogs)—advancing beyond earlier whole-body mean dose calculations by Lange et al. (28).

Recent work has leveraged the auger electrons emitted from ¹⁹¹Pt towards targeted therapy. Obata et al. (29) developed a resin-based method to isolate n.c.a. [188,189,191Pt(II)Cl₄²⁻, and a one-pot radiosynthesis of [*Pt]cisplatin, yielding 30%-40% without intermediate evaporation. Using tracer-level [189,191Pt] cisplatin, Obata et al. (30) showed only 0.6% overall cell uptake in cells, yet ~20% of internalized platinum localized to the nucleus and \sim 2% bound covalently to DNA (0.28 \pm 0.02% ID/ mg) (30). Single-cell assays confirmed that auger electrons caused direct DNA double-strand breaks, validating [189,191Pt] cisplatin as an extremely localized therapeutic with minimal systemic toxicity (30). Obata et al. (31) compared ¹⁹¹Pt coordination to Cys, DTPA, EDDA (Figures 1B-D) to evaluate the *in vitro* behavior to analogous 111 In-labeled ($t_{1/2} = 2.8$ d, 100% EC) agents (31-34). They demonstrate that free ¹⁹¹PtCl₄²⁻ undergoes rapid thiol coordination with Cys, significantly reducing protein binding at 60°C (~10%) compared to 45°C (~42%) (31). In contrast, labeling with DTPA and EDDA resulted in moderate radiochemical yields (70%–80%) and reduced protein binding only to ~42% and ~30%, respectively (31). Furthermore, ¹⁹¹Pt was complexed with the DNA-targeting dye Hoechst33258 via DTPA ([¹⁹¹Pt]Pt-DTPA-Hoechst33258; >95% radiochemical purity) and Cys ([¹⁹¹Pt]Pt-Cys-Hoechst33258; ~90% radiochemical purity) to compare with [¹¹¹In]In-DTPA-Hoechst33258 (>95% radiochemical purity) and found both ¹⁹¹Pt-based complexes displayed one order of magnitude greater DNA-binding than the ¹¹¹In analog (31). Notably, [¹⁹¹Pt]Pt-Cys-Hoechst33258 induced DNA damage more effectively than its DTPA counterpart, suggesting that thiol-based ¹⁹¹Pt labeling enhances delivery to DNA and elevates therapeutic potential (31).

Obata et al. (35) conjugated 191Pt to a oncogene MYCNspecific pyrrole-imidazole polyamide (PIP) scaffold (191Pt-MYCN-PIP) bearing Cys, tri-arginine (R3) for cellular penetration (36), and a fluorescent compound coumarin (GCC-Cys-R3-coumarin control, 191Pt-GCC-PIP). The MYCN gene is a transcription factor that is amplified in human neuroblastoma and is related to the patient's prognosis (35). Noted in Obata et al. (35), targeting cancer-related genes with PIPs have been utilized in preclinical studies with mice and marmosets (37, 38), along with developments of MYCN-targeting PIP in Yoda et al. (39) showed promising specific targeting ability and therapeutic effects. With 50%-70% radiochemical yield and >95% radiochemical purity, 191Pt-MYCN-PIP achieved ~10-fold higher uptake and DNA-binding in MYCN-amplified vs. non-amplified neuroblastoma cells, and reduced MYCN expression in vitro (35). Omokawa et al. (40) synthesized a sugar-conjugated platinum complex, FGC-Pt (cis-dichloro[(2-fluoro-α-_Dglucopyranosidyl)propane-1,3-diamino-2-propyl]platinum) (41) and labeled it with n.c.a. ¹⁹¹Pt by either direct activation (61.7% radiochemical purity) or post-labeling of neutron-activated [191Pt]K₂PtCl₄ $(14.5 \pm 7.3\%$ radiochemical yield; radiochemical purity), with the latter method providing significantly higher yield and purity. In healthy mice, both [¹⁹¹Pt]FGC-Pt preparations showed almost biodistribution at 24 h—and γ-counting correlated with ICP-MS measurements (r = 0.92, p < 0.05), confirming their utility for quantitative imaging (40). Most recently, Obata et al. (42) developed a PSMA-targeting 191Pt-trithiol complex showing a 46-fold uptake advantage in PSMA+ vs. PSMA- tumors (in vitro), outperforming the Cys-based analog (2.2 ± 0.3) .

2.2 Platinum-193 m, 193mPt

Platinum-193 m is a metastable isomer of platinum-193 that may be useful for Auger electron therapy. This radionuclide is attractive due to emitting around 26 Auger electrons per decay and has a half-life of 4.33 days (43).

2.2.1 Production and radiochemical separation of ^{193m}Pt

The production routes to obtain ^{193m}Pt are shown in Table 1. Uddin et al. (44) measured the experimental excitation function

FIGURE 1

A select subset of a ¹⁹¹Pt complex and chelators discussed in this section are highlighted. (A) The chemotherapy agent, *cis*-diamminedichloroplatinum(II) (cisplatin) is widely used in the treatment of various forms of carcinomas and sarcomas, which was radiochemically synthesized with ¹⁹¹Pt ([¹⁹¹Pt]-cisplatin) for investigation (25–28, 30). The complex is represented as elemental platinum. Obata et al. (31) compared ¹⁹¹Pt coordination to (B) amino acid cysteine (Cys), and both multidentate chelators, (C) ethylenediaminediacetic acid (EDDA) and (D) diethylenetriaminepentaacetic acid (DTPA).

for the ¹⁹²Os(α,3n)^{193m}Pt reaction—building on previous work by Hilgers et al. (45)—reporting a peak cross section of 1.47 ± 0.19 b (66.63 keV x-ray) and 1.53 ± 0.21 b (135.5 keV γ -ray), both at 36.4 ± 0.2 MeV. As the authors noted, several methods for the dissolution of osmium had been reported (45-47). An optimized electrolytic technique was carried out to prepare highly enriched ¹⁹²Os, where the authors noted, low electrodeposition yields were minimal to this point (44). Jones et al. (48) reported a maximum deposition of 9.5% at pH 13-which encouraged the authors to focus on this effort. Chakrabarty et al. (47) on the other hand, reported a high yield of ~80% for an isotopically enriched osmium sample, where efforts by Uddin et al. (44) were devoted to optimizing the electrolytic deposition process. By using their electrolyte, a maximum electrodeposition yield of ~75% at pH 12.8 was achieved for the enriched osmium, with 15% lower for natural osmium. Adopting radiochemical separation techniques from Bonardi et al. (21) and Hilgers et al. (45), Uddin et al. (44) oxidized the osmium sample with the Ni backing in concentrated nitric acid and evaporated out the liquid. The OsO₄ was distilled and trapped in 4.7 N KOH, while the residual Pt was dissolved in 3 N HCl, and reduced from Pt (IV) to Pt(II) with $SnCl_2$. The $[Pt(SnCl_3)_5]^{3-}$ anion was extracted into the ether phase, achieving a radiochemical yield of 80%-96% across 20 individual osmium samples (44). Compared to Hilgers et al. (45) and predictions from nuclear model codes [TALYS (49) and STAPRE (50)], the measured excitation functions from (44) showed excellent agreement across the energy range. Integral yield calculations 1 µA for 1 h yielded ~10 MBq/μA-h of 193mPt and ~0.06 MBq/μA-h of $^{195\text{m}}\text{Pt}$ within the optimal energy window of $40{ o}30~\text{MeV}$, establishing $^{192}Os(\alpha,3n)^{193m}Pt$ as the most effective cyclotronbased route for producing clinically relevant quantities of ^{193m}Pt (44).

Uddin et al. (51) demonstrated a small-scale, cyclotron-based production of $^{193\text{m}}$ Pt via $^{192}\text{Os}(\alpha,3\text{n})^{193\text{m}}$ Pt reaction, achieving 99% radionuclidic purity and a specific activity of 1 GBq/µg $^{193\text{m}}$ Pt, effectively overcoming the limitations of low specific activity associated with reactor-based (n, γ) production on 192 Pt targets as highlighted by Azure et al. (52). Target dissolution and OsO₄ distillation, previously reported in Hilgers et al. (45)

and Uddin et al. (44), combined with a SnCl2-ether extraction sequence developed by Ahmed and Koch (53) and Koch and Yates (54), enabled 85% recovery of enriched Os and 90% radiochemical yield of ^{193m}Pt (51). The experimental batch yield at EOB was ~10 MBq using a 1.6 μA beam for 3 h, corresponding to ~40% of the theoretical value predicted from the excitation function of the $^{192}\mathrm{Os}(\alpha,3n)^{193m}\mathrm{Pt}$ reaction (44, 51). In contrast, (n,γ) production using 5 mg of 57% enriched 192 Pt ($\phi = 4 \times 10^{14} \text{ n cm}^{-2} \text{ s}^{-1}$; 7 d) yielded 3 GBq with a specific activity of only 0.6 MBq/ μg ^{193m}Pt (51, 52). Moreover, α induced production results in minimal ^{195m}Pt impurity (0.5%) compared to the (n,γ) route (~12%), emphasizing its suitability high-purity Auger-electron scalable, radionuclide production (51, 52).

2.2.2 Applications of ^{193m}Pt

Lange et al. (55) performed the radiosynthesis of cisplatin labeled with 193mPt and subsequent biodistribution on rabbits and mice. From their findings following intravenous injection, most of the activity accumulated in the kidneys, urine, and liver, with rapid excretion of the radiolabeled complex (79% eliminated by 24 h) (55). A year later, the same group (28), performed distribution studies and dose calculations for 193mPt and 195mPt and reported similar biodistribution results from the prior study, along with similar behavior with the ^{195m}Pt-labeled analog (28). Azure et al. (52) performed the first microscale synthesis of carboplatin labeled with ^{193m}Pt, reporting [^{193m}Pt] carboplatin (Figure 2) uptake had saturated by 2-3 in V79 cells, and similar findings to [195mPt]transplatin in Howell shown in Figure 3A (56). Notably, ~70% of internalized ^{193m}Pt was in the nucleus, with ~60% of that bound to DNA (52)—substantially higher targeting than observed with 195mPt (25% cellular radioactivity in nucleus, 42% bound to the DNA) (56).

2.3 Platinum-195 m, ^{195m}Pt

Owing to its favorable nuclear decay properties, ^{195m}Pt has been studied for its use in both nuclear medicine diagnosis and therapy. The radionuclide has a half-life of 4.02 d, emits low-

$$H_3N$$
 Pt O O

FIGURE 2

An analog of cisplatin, *cis*-diammine(1,1-cyclobutanedicarboxylato)-platinum(II) (carboplatin, paraplatin[®]) has demonstrated to strongly diminish renal toxicity and other associated deleterious physiological phenomena, along with clearance of the drug from the body is much faster than for cisplatin (52). We present the complex structure using elemental platinum; however, Azure et al. (52) radiochemically synthesized carboplatin with ^{193m}Pt (1^{93m}Pt) carboplatin) (52).

energy photons (E_{γ} = 98.85 keV, I_{γ} = 11.4%), each disintegration releases 36 Auger electrons depositing around 25 keV within nm- μ m distances in tissue (57, 58).

2.3.1 Production and radiochemical separation of ^{195m}Pt

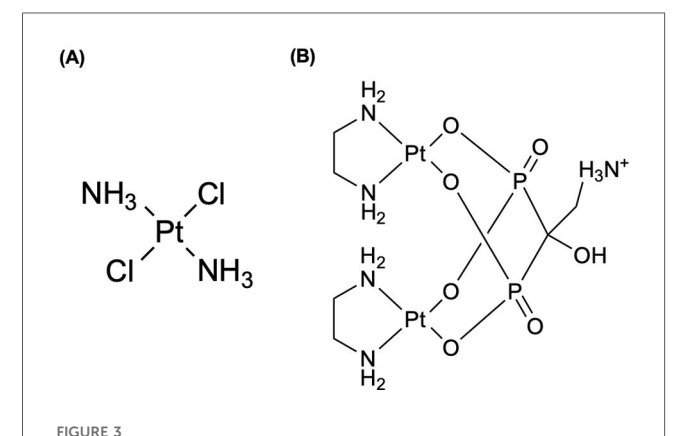
High specific activity 195mPt is best obtained via indirect reactor routes or enriched target irradiation, and all its production routes are shown in Table 1. Knapp et al. (59) produced n.c.a. 195mPt by irradiating enriched 193Ir to produce 195m Ir $(t_{1/2} = 3.67 \text{ h})$ —via 193 Ir $(n,\gamma)^{194}$ Ir $(n,\gamma)^{195m}$ Ir—which then decays (β^-) to $^{195 \mathrm{m}}$ Pt while taking advantage of the high thermal flux of the High-Flux Isotope Reactor (HFIR) at Oak Ridge National Laboratory (ORNL) to surpass the specific activities achievable by direction 194 Pt(n, γ) or 195 Pt(n,n') routes (26, 59, 60). 195mPt was separated from bulk Ir via thiourea-HCl elution on cation resin-where methods were previously reported by Siegfried et al. (61) and Berg and Senn Jr (62).yielding high purity of 195mPt (59). Hilgers et al. (45) measured the ¹⁹²Os(α,n)^{195m}Pt reaction, reporting a maximum cross section of 4.4 ± 0.7 mb at 22.1 ± 0.7 MeV, and projected ~ 0.09 GBq yield—about an order of magnitude lower than reactor methods (63). Vosoughi et al. (64) irradiated natPt in a reactor $(3 \times 10^{13} \text{ n cm}^{-2} \text{ s}^{-1}, 30 \text{ h}, 5 \text{ MW power})$, obtaining 16.28 MBq of 195mPt. The product was allowed to decay for 48-h due to short-lived Au/Pt impurities and solvent extraction separation was performed following an established method by Vimalnath et al. (65), they obtained radiochemical yield and separation efficiency of ≥99% and 99.4%, respectively (64). However, specific activity was only ~0.8 MBq/mg, much lower compared to the reported <37 MBq/mg (59) and 15.9 MBq/mg (66) that were achieved with enriched 194Pt targets at ORNL and SAFARI-1 reactors, respectively (64). Bodnar et al. (67) aimed to develop a method of preparation of 195mPt with high specific activity via a photonuclear reaction. Obtaining 195mPt via the ¹⁹⁷Au(γ,np)^{195m}Pt reaction, they implemented a novel technique for gold extraction and produced high specific activity 195mPt >1 Ci/mg (67). Wawrowicz and Bilewicz (57) tested the doubleneutron capture approach but proved it to be impractical due to an unknown second-step cross section and difficult target dissolution, yielding <10% recovery. Therefore, until nuclear data and chemical processing improves, double-capture routes offer no advantage (57).

2.3.2 Applications of ^{195m}Pt

Leveraging reactor-produced n.c.a. 195mPt, Zeevart et al. (66) prepared [195mPt]cisplatin for a Phase 0 clinical trial on healthy patients (66). Using an optimized synthesis—building on work by Smith (68)-[195mPt]cisplatin was obtained in >95% radiochemical yield (195mPt and 197Pt combined), with coproduced impurities (192Ir, 191Pt, Au isotopes) below detection (66). Sathekge et al. (69) obtained whole-body planar scans and SPECT/CT images up to 144 h post-[195mPt]cisplatin injection in five volunteers. Bodnar et al. (67) also optimized the radiosynthesis of 195mPt-cisplatin from earlier works of Chernyaev (70) and Dykiy et al. (71) for in vitro and in vivo evaluation. They confirmed induced necrosis and apoptosis in vitro at mass doses over five orders of magnitude lower than conventional cisplatin doses (67, 70, 71). In mice with Ehrlich tumors, a single [195mPt]cisplatin dose achieved 65% tumor growth inhibition—and 100% animal survival—vs. 35% inhibition by conventional cisplatin (67).

Apart from cisplatin analogs, Aalbersberg et al. (72) conducted a preclinical evaluation of 195mPt SPECT using NanoSPECT/CT and U-SPECT+/CT scanners following thermal neutron irradiation of 194Pt in the High Flux Reactor (HFR) in Petten, the Netherlands. They achieved sub-millimeter resolution and linear quantification over a wide activity range (0.035-4.36 MBq), confirming accurate in vivo Pt distribution measurements (72). SPECT-based quantification, calibrated using a 195mPt dilution series, correlated strongly with ex vivo gamma-counting and graphite-furnace atomic absorption (GF-AAS), validating accurate quantification of platinum biodistribution (72). Although the study validated the feasibility of 195mPt SPECT in small animals, the authors noted limitations including low specific activity 3-4 MBq per injection, small sample size, and the need to improve purification methods to extend imaging with radiolabeled cisplatin (72). Muns et al. (73) characterized a metal-organic linker, $[ethylenediamineplatinum(II)]^{2+}$ (called Lx) with antibody-drug conjugates (ADCs) for in vivo stability and tumor targeting using 195m Pt and 89 Zr ($t_{1/2}$ = 78.36 h). Nearly identical ^{195m}Pt and ⁸⁹Zr biodistributions in tumor-bearing mice confirmed the in vivo stability of the Pt(II)-histidine coordinative bond within Lx (73). However, the amounts of platinum incorporated into Lx-based ADCs and the specific activity of ^{195m}Pt were too low to support preclinical or clinical SPECT imaging studies (73).

Nadar et al. (74) synthesized a n.c.a 195m Pt-BP complex, shown in Figure 3B, to achieve bone-targeting Auger-electron therapy. This complex was introduced previously by Margiotta et al. (75). In healthy C57BL/6N mice (2.5 mM Pt, 24 h), ICP-MS showed a 4.5-fold higher uptake in hard tissue (12.18 \pm 0.56%ID/g) vs. its bisphosphonate-free precursor Pt(NO₃)₂(en) (2.69 \pm 0.26%ID/g),



(A) The complex of *trans*-dichlorodiammineplatinum(II) (transplatin) was radiochemically synthesized with radioactive platinum (I^{195m}Pt]-transplatin) in Howell et al. (56) to be utilized as an antitumor drug (56). (B) Radioactive bisphosphonate-functionalized platinum (^{195m}Pt-BP) complexes were investigated to specifically accumulate in intratibial bone metastatic lesions in mice (74–76). Both complexes are presented as elemental platinum.

and accomplished reducing off-target retention in many organs including the kidney $(5.70 \pm 0.15 \text{ vs. } 3.38 \pm 0.28\%\text{ID/g})$ (74). Pt-BP also induced minimal Pt-DNA adduct formation (<0.5% of total Pt in most tissues; kidney: 2.8%, spleen: 1.4%) compared to the precursor (kidney: 4.8%, spleen: 9.8%), confirming that bisphosphonate conjugation both enhances bone selectively and spares healthy tissues for DNA damage (74). In micro-SPECT/ CT studies, 195mPt-BP rapidly localized to growth plates, whereas ^{195m}Pt(NO₃)₂(en) accumulated specifically in soft tissues (74). Laser ablation ICP-MS (LA-ICP-MS) further validated 73.5% co-localization of 195mPt-BP, showing almost a four-fold increase accumulation of Pt in bone compared to the precursorhighlighting its specific bone-binding mechanism (74). In a subsequent study, Nadar et al. (76) treated mice with intratibial bone tumors using 195mPt-BP and [195mPt]cisplatin. 195mPt-BP exhibited significantly higher and sustained accumulation in metastatic lesions with 2.8-3.3-fold higher uptake than the contralateral tibia, indicating selective targeting (76). In contrast, ^{195m}Pt-cisplatin exhibited lower uptake (≤3.7%ID/g) with no evidence of lesion selectivity at any time point (76). Therapeutic efficacy was assessed via γ-H2AX staining—a biomarker specific for double-strand DNA breaks—revealing that 195mPt-BP induced a 4.6-fold greater fraction of γ-H2AX-positive tumor cells $(1.66 \pm 0.4\%)$ compared to 195m Pt-cisplatin $(0.36 \pm 0.1\%)$ and an 11-fold increase over non-radioactive Pt-BP $(0.15 \pm 0.1\%)$ (76). These results confirm that bone-targeted ^{195m}Pt-BP delivers Auger radiation directly to tumor-associated bone lesions with superior efficacy compared to [195mPt]cisplatin (76).

Most recently, de Roest et al. (77) explained [195mPt]cisplatin uptake in cisplatin-sensitive and -resistant head-and-neck cancer models. They found that cisplatin-resistant HNSCC cell line (VU-SCC-OE) accumulated more [195mPt]cisplatin in DNA and exhibited greater capacity to repair cisplatin-induced crosslinks compared to the cisplatin-sensitive HNSCC cell line (VU-SCC-1131), with a DNA retention ratio of 3.4 vs. 1.45 (77). The

authors concluded that [^{195m}Pt]cisplatin imaging is not predictive of tumor sensitivity to cisplatin but may serve as a tool for assessing cisplatin-related off-target toxicity (77).

3 Palladium and palladium-based radionuclides

There are six naturally occurring stable isotopes of palladium: $^{102}\mathrm{Pd}$ (1.0%), $^{104}\mathrm{Pd}$ (11.0%), $^{105}\mathrm{Pd}$ (22.2%), $^{106}\mathrm{Pd}$ (27.3%), $^{108}\mathrm{Pd}$ (26.7%), and $^{110}\mathrm{Pd}$ (11.8%) (19). Radioisotopes of palladium include $^{100}\mathrm{Pd}$, $^{103}\mathrm{Pd}$, $^{107}\mathrm{Pd}$, and $^{109}\mathrm{Pd}$, in this review we will discuss $^{103}\mathrm{Pd}$ and $^{109}\mathrm{Pd}$.

3.1 Palladium-103, ¹⁰³Pd

 103 Pd ($t_{1/2}$ = 16.99 d) is a therapeutic radionuclide that has been used in brachytherapy for the treatment of prostate cancer, mostly used as a metal seed or stent (78, 79). The radionuclide decays to 103 mRh by electron capture, which then de-excites through internal transition (IT) to stable 103 Rh. 103 Pd emits x-rays and Auger electrons due to the EC and IT decays, which makes 103 Pd suitable for internal radiotherapy (79).

3.1.1 Production and radiochemical separation of $^{103}\mathrm{Pd}$

A variety of production methods exist for ¹⁰³Pd, including reactor- and accelerator-based routes which is described in Table 2. Sudar et al. (80) reported a maximum cross-section of 505 ± 26 mb at 10.05 ± 0.19 MeV (via x-ray measurements) and identified the optimal energy range for maximizing specific cross-sections (300–500 mb) and yields to be between 8 and 12 MeV. The authors compared between neutron-counting studies—including those by Albert (81), Johnson et al. (82), and Hansen and Albert et al. (83)—and activation measurements—Blaser et al. (84), Harper et al. (85), Treytl and Caretto (86), Mukhammededov and Vasidov (87), and Hermanne et al. (88)—from energies 2.8–400 MeV, confirming good agreement across studies, with discrepancies at lower energies mainly

TABLE 2 Production pathways for palladium-based radionuclides.

Radionuclide	Nuclear reaction	Flux/Energy	References
¹⁰³ Pd	natAg(p,x)103Pd	$E_{max} = 100 \text{ MeV}$	(79, 89-91)
	¹⁰³ Rh(p,n) ¹⁰³ Pd	E _{max} = 50 MeV	(79, 80, 101, 102)
	¹⁰³ Rh(d,2n) ¹⁰³ Pd	E _{max} = 34 MeV	(79, 92, 93, 99)
	100 Ru(α ,n) 103 Pd	25 → 9 MeV	(79, 94, 95)
	101 Ru(α ,2n) 103 Pd	25 → 15 MeV	(79, 94, 95)
	¹⁰² Ru(³ He,2n) ¹⁰³ Pd	34 → 7 MeV	(79, 94, 95)
	$\begin{array}{c} ^{nat}Pd(d,xn)^{103}Ag \rightarrow \\ ^{103}Pd \end{array}$	$E_{\text{max}} = 20.5 \text{ MeV}$	(95, 98)
	${\overset{nat}{^{103}}} Pd(p,x){\overset{103}{^{103}}} Ag \rightarrow$	$E_{\text{max}} = 37.3 \text{ MeV}$	(79, 97, 98)
¹⁰⁹ Pd	¹⁰⁸ Pd(n,γ) ¹⁰⁹ Pd	$3 \times 10^{13} \text{ n cm}^{-2}$ s^{-1}	(78, 123)

attributing to systematic uncertainties and differences in target preparation (80). Building on this, Hussain et al. (79) provided a comprehensive evaluation of all accelerator-based production routes for n.c.a. 103 Pd, integrating six reaction channels (89–95) reported in Table 2 using EXFOR data and key literature sources, and by normalizing the raw measurements with three nuclear-reaction codes (STAPRE (50), TALYS (49), and EMPIRE (96)) to produce recommended excitation functions with 95% confidence limits. Furthermore, they investigated another indirect precursor of $^{\rm nat}$ Pd(p,x) $^{\rm 103}$ Ag \rightarrow $^{\rm 103}$ Pd (97, 98) that can form up to 70% of total $^{\rm 103}$ Pd via $^{\rm 103}$ Ag decay but suffers from long-lived impurities and complex chemistry, limiting their large-scale clinical applicability (79).

Manenti et al. (99) optimized n.c.a. 103Pd production via the 103Rh(d,2n) reaction using a stacked-foil activations method at deuteron energies from 5 to 33 MeV on the JRC-Ispra and ARRONAX cyclotrons (beam currents 100-170 nA, 1 h irradiations). Experimental cross-sections rose steadily above the 3.62 MeV threshold, peaking at $1,261 \pm 71$ mb at 15.0 ± 0.4 MeV, and then declined gradually at higher energies (99). Comparison with prior data and models showed good agreement with Hermanne et al.'s (92) γ-ray measurements and close agreement with the recommended values of Hussain et al. (79), while Ditroi et al. (100) reported cross-sections up to 15% lower (99). Furthermore, EMPIRE-II and EMPIRE-3.2.2 (96) both reproduced the experimental curve within uncertainty, whereas TENDL-2015 (49) underestimated cross-sections above 10 MeV (99). Thick-target yields (TTYs) were computed from integrated thin-foil data, reporting that up to ~12 MeV, deuteron-induced TTYs matched those of the 103Rh(p,n) route (99). Above 12 MeV, deuteron yields exceed proton yields by up to a factor of two-reflecting the higher (d,2n) cross-section at medium energies and marking deuteron beams as especially attractive for high-throughput production (99). Radionuclidic purity within the 5-33 MeV window is excellent as authors noted only ¹⁰¹Pd $(t_{1/2} = 8.47 \text{ h})$ co-produces above its 22 MeV threshold, greatly simplifying post-irradiation separation (99). The higher stopping power of 13.3 MeV deuterons also reduces target mass, with a 188 μm Rh foil suffices for full absorption vs. 214 μm for 10.5 MeV protons, marginally easing radiochemical separation (99). Despite these advantages, high-energy deuteron cyclotrons remain scarce, which may constrain routine clinical-scale 103Pd production (99).

Ohya et al. (101) demonstrated an efficient method for producing no-carrier-added 103 Pd, followed by radiochemical separation and target material recycling. The radiochemical separation incorporated a Bi-Rh alloying pretreatment at 500°C, enabling high-yield dissolution of the Rh target and achieving a 93 \pm 4% dissolution efficiency (101). Following co-precipitation to remove Bi and palladium radionuclides—including 100 Pd and 103 Pd— a dimethylglyoxime (DMG)-based extraction, achieved 99 \pm 1% yield (101). The radiopalladium was subsequently back-extracted from chloroform using aqueous ammonia, yielding 97 \pm 2% of $[^{103}$ Pd(NH₃)₄]²⁺ (101). The entire process was completed within 3.5 h, yielding a 103 Pd radiochemical yield of 87% and >99% radionuclidic purity (101). During the recycling

process, $91\pm3\%$ of the Rh target was efficiently recovered with minimal Bi contamination (9 µg per 50 mg Rh) through cation exchange purification; therefore, providing a framework for clinical-scale ¹⁰³Pd radionuclide production (101).

Krol et al. (102) presented the first feasibility study on the production of 103Pd via the 103Rh(p,n)103Pd reaction using cyclotron irradiation of a liquid target. By achieving an EOB activity of 1.03 ± 0.05 MBq $(20.06 \pm 0.97$ MBq/ μ A) under optimized conditions $(30 \pm 0.5 \,\mu\text{A}, 1 \,\text{h})$ irradiation, 200 psi top up pressure, and 16.4 mg/ml metal-salt concentration), they demonstrated that liquid targets can reliably yield research-scale quantities of 103Pd suitable for radiochemistry (102). Furthermore, an anion-exchange separation using Dowex 1×8 resin with 1 M HNO₃ for rhodium elution achieved a $90.1 \pm 2.1\%$ recovery from the irradiated target solution, while a 1:1 mixture of 0.5 M NH₃ + NH₄Cl for palladium elution resulted in a 103.8 ± 2.3% recovery—achieving a rhodium reduction factor of $\sim 10^6$ (102). More recently, Laouameria et al. (103) addressed previous limitations by developing a diffusiondriven extraction to separate 103Pd from its stable 103Rh target, relying on the metals' differing vapor pressures. Using their radionuclide separation equipment (RSE), they achieved an overall separation of $17 \pm 2\%$ and deposition yields of $77 \pm 2\%$ on Nb foil and $49 \pm 2\%$ on ZnO/W discs, respectively (103). Furthermore, using the ZnO/W disc substrate, the method produced 31.9 MBq EOB with a specific activity of 8.1 GBq/g, representing a streamlined alternative to traditional wetchemistry approaches for Auger-emitter production (103).

3.1.2 Applications of ¹⁰³Pd

Blasko et al. (104) conducted a study on a cohort of 230 men with clinically T1-T2 prostate cancer treated exclusively with ¹⁰³Pd brachytherapy. The study found an overall 9-year biochemical control rate of 83.5%, with PSA-only progression observed in just 4.3% of patients (104). The findings validated ¹⁰³Pd brachytherapy as an effective and durable treatment option cross a range of risk groups, achieving high biochemical and clinical outcomes in patients with organ-confined prostate cancer (104).

Li et al. (105) developed an electroless plating method to fabricate ¹⁰³Pd brachytherapy seeds by directly depositing ¹⁰³Pd onto carbon bar substrates, thereby eliminating the metallic precoatings and the complex pellet assemblies required from prior reports. Under hydrazine-based bath conditions optimized in Li et al. (106), this method achieves a 98% deposition efficiency and a ¹⁰³Pd utilization rate of 51%, which is more than double (~25%) seen with traditional silver bars (105). By streamlining the plating process and cutting material losses, the approach reduces both fabrication cost and complexity, paving the way for more economical, high-performance ¹⁰³Pd seed production and broader clinical adaptation (105).

Researchers have also explored ¹⁰³Pd in nanoparticle-based brachytherapy. Laprise-Pelletier et al. (107) evaluated the therapeutic efficacy, biodistribution, and tolerability of two formulations of ¹⁰³Pd-doped Pd@Au nanoparticles (NPs) in a prostate cancer xenograft model. Like Djoumessi et al. (108), the Pd NP synthesis achieved a high encapsulation efficiency of 87%

for all ¹⁰³Pd atoms incorporated into the 10-14 nm cores (107). Comparing to Moeendarbari et al. (109), who reported 80% tumor inhibition after a 1.5 mCi implant given in 40 µl, the present study achieved similar therapeutic effects using a tenfold smaller volume (4 μl at 1.6–1.7 mCi) (107). Fach et al. (110) formulated 103Pd within gold-palladium (AuPd) alloy nanoparticles, intrinsically radiolabeled with 103Pd, capable of forming biodegradable gel-like implants upon injection. Therapeutic efficacy of ¹⁰³Pd-nanogels in a tumor-bearing mouse model indicated doses of 25 MBq [103Pd]AuPd-nanogel produced a robust tumor-growth delay and double median survival compared to controls, with no systemic toxicity (110). Building on this, Sporer et al. (111) compared injectable ¹⁰³Pdbrachytherapy seeds that form biodegradable LOIB-based solids in situ, using either intrinsically radiolabeled PdAuNPs or a novel SSIB-[16]aneS4 chelator. The [103Pd]PdAuNPs were synthesized by co-reduction of [103Pd]PdH2Cl4 and AuHCl4 surface-functionalized with a lipophilic coating and dispersed in LOIB:EtOH to achieve an overall radiochemical yield of 83% or via conjugation of the [16]aneS4 chelator shown in Figure 4A to a lipophilic sucrose septaisobutyrate (SSIB), followed by complexation with [103Pd]PdH2Cl4 in 99% yield (111). While both formulations reached activities of 1-1.5 GBq/ml with negligible release (<1%) of radioactivity over 30 days, the chelator strategy deems to be favorable as it avoids nondegradable gold and offers a versatile platform for other radiometals (111).

Hindie et al. (112) used the Monte Carlo track-structure code CELLDOSE (113) (for electrons) in conjunction with PHITS (114) (for photons) to quantify energy deposition from ¹⁰³Pd/^{103m}Rh at the cell surface, within the cytoplasm, and in the nucleus enabling normalized comparison against ¹⁶¹Tb and ¹⁷⁷Lu. In the single-cell

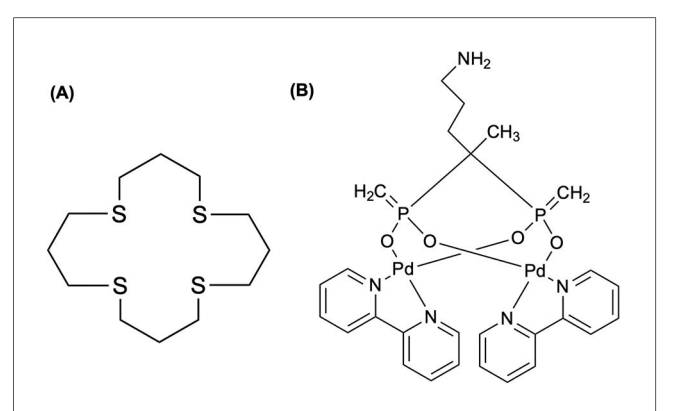


FIGURE 4(A) A tetradentate thioether macrocycle, 1,5,9,13-tetrathiacyclohexadecane ([16]aneS₄), has been a suitable chelator for binding Pt(II) and Pd(II) complexes. The chelator has been used to immobilize ^{103}Pd in a ^{103}mRh generator (118), where Sporer et al. (111) coupled [16]aneS₄ to sucrose septaisobutyrate (SSIB) moiety, furnishing a ligand capable of efficiently trapping ^{103}Pd within the lactose octaisobutyrate (LOIB) seed. (B) The elemental palladium complex with bipyridyl and alendronate ligands, Pd₂(bpy)₂ale, was radiochemically synthesized with ^{103}Pd and ^{109}Pd for radionuclide therapy of bone metastatic tumor cells (115).

model, 103Pd delivered 7- to 10-fold higher nuclear absorbed dose and 9- to 25-fold higher membrane dose than 177Lu-driven primarily by Auger and conversion electrons—with 161Tb showing intermediate dose profiles (112). Annamalaisamy et al. (115) reported the first radiosynthesis and evaluation of ¹⁰³Pd₂(bpy)₂ale (Figure 4B), designed as an in vivo ¹⁰³Pd/^{103m}Rh generator for bone-targeted Auger-electron therapy—extending prior work by Cipriani et al. (116) and Fathy et al. (117). At pH of 7 and 60°C, the radiosynthesis achieved >85% radiochemical yield by iTLC, and preparative HPLC confirmed radioactive and non-radioactive complexes were identical (115). Notably, iTLC showed complete retention of parent 103Pd and daughter 103mRh —significantly improving upon macrocyclic ¹⁰³Pd/^{103m}Rh generators reported by Jensen et al. (118), which exhibited ~7% ^{103m}Rh release—related to the electron-donating bipyridyl ligand quenching "Coulomb explosion" effect discussed in Nath et al. (115, 119). The result from the work of Jensen et al. (118) can be explained by works of van Rooyen et al. (120) and Szucs et al. (121) who conducted detailed recoil energy calculations associated with the emission of Auger electrons, photons, and neutrinos (115). Finally, ¹⁰³Pd₂(bpy)₂ale exhibited potent multimodal toxicity via Auger electrons and demonstration chemotoxicity comparable to cisplatin by works of Zhao et al. (122), highlighting its theragnostic potential (115).

3.2 Palladium-109, ¹⁰⁹Pd

¹⁰⁹Pd ($t_{1/2}$ = 13.7 h) possesses favorable nuclear characteristics suitable for targeted radionuclide therapy and SPECT imaging as it decays by β^- emission ($E_{\beta(\text{max})}$ = 1.12 MeV, 100%) to ^{109m}Ag ($t_{1/2}$ = 39.6 s), which then emits an 88 keV photon (I_{γ} = 3.6%) before it finally decays to ¹⁰⁹Ag, from a cascade emission of both conversion and Auger electrons (123). As described in Boros and Packard (78), the radionuclide was originally proposed for radiolabeling of antibodies for antitumor therapeutic purposes, but the focus has changed to exploring ¹⁰⁹Pd-porphyrin complexes as photosensitizing agents for photodynamic therapy of cancer (78). Fawwaz et al. (124) first demonstrated the anticancer capabilities of ¹⁰⁹Pd by labeling hematoporphyrin and protoporphyrin for controlling homograft rejection (125).

3.2.1 Production and radiochemical separation of ¹⁰⁹Pd

Highlighted in Table 2, 109 Pd is produced using an enriched 108 Pd (98%) metal target, which was performed by Chakraborty et al. (123), obtaining a specific activity of \sim 1.85 GBq/mg (50 mCi/mg) at a thermal neutron flux of 3×10^{13} n cm $^{-2}$ s $^{-1}$ for 3 days (78). In the review by Boros and Packard (78), a dissolution method is carried out in heated aqua regia and is subsequently evaporated and heated to dryness with 12 N HCl to form $\rm H_2PdCl_4$. Silver-111 (111 Ag) is co-produced and can be removed by coprecipitation with small amount of AgNO₃ (78). The supernatant containing 109 Pd is later dissolved in dimethylsulfoxide (DMSO) to produce 109 Pd(DMSO)₂Cl₂ for subsequent syntheses (78). Hien et al. (126) reported thermal

neutron capture cross-section (σ_0) and resonance integral (I_0) of the $^{108}\text{Pd}(n,\gamma)^{109}\text{Pd}$, backing previous work of thermal neutron capture cross sections (127–134) and resonance integral data (131, 135) for this reaction.

3.2.2 Applications of ¹⁰⁹Pd

Porphyrin derivatives are well known to preferentially accumulate in malignant tumors via photodynamic mechanisms (136-139), and early efforts to radiolabel these macrocycles with therapeutic radionuclides—such as ¹⁰⁹Pd-hematoporphyrin (140) ¹⁰⁹Pd-antimelanoma antibodies (141)—demonstrated targeting potential but lacked tumor retention. To expand upon this potential, Das et al. (142) radiolabeled a porphyrin derivative (DHBEP) with n.c.a. 109Pd to create a highly stable, rapidly tumor-localizing radiopharmaceutical. The novel ligand DHBEP was synthesized via a two-step sequence and complexed with 109PdDMSO₂Cl₂ at 80°C for 1 h, achieving >98% radiochemical purity. The 109Pd-DHBEP complex remained stable at >97% after 48 h (~4 half-lives of 109Pd) at room temperature in saline (142). Biodistributions studies with Swiss mice bearing fibrosarcoma tumors revealed high tumor uptake at 30 min p.i. $[(5.28 \pm 1.46\%IA/g)]$ and activity was cleared via the renal pathway (142).

Pineau et al. (125) evaluated TE1PA, shown in Figure 5, to demonstrate its suitability for complexation with both natural and radioactive palladium towards radiopharmaceutical development. Under all conditions and comparing TE1PA to cyclam, TE1Bn (benzyl cyclam), TE1Py (pyridylmethyl cyclam), they reported significant improvement in inertness of [109Pd] [Pd(TE1PA)]⁺ over [109Pd][Pd(cyclam)]²⁺ at room temperature over a 24-h period, highlighting the enhances properties of the picolinate derivative (125).

Gharibkandi et al. (143) developed ¹⁰⁹Pd-coated gold nanoparticles (Au@¹⁰⁹PdNPs) functionalized with polyethylene glycol (PEG) conjugated to trastuzumab for targeted therapy of HER2-positive cancers. The resulting Au@Pd-PEG-trastuzumab

FIGURE 5

A monopicolinate cyclam, TE1PA, was developed by (255–258) as it exhibited improved properties for $^{64}\text{Cu}\text{-immuno-PET}$ imaging in terms of radiolabeling yield, conjugation to those of DOTA and NOTA derivatives (125). Pineau et al. (125) investigated the coordination of the chelator with elemental Pd and ^{109}Pd to assess the potential development of theragnostic pairs of either $^{64}\text{Cu}/^{103}\text{Pd}$ or $^{64}\text{Cu}/^{109}\text{Pd}$.

radiobioconjugate averaged 9.5 antibodies per nanoparticle and demonstrated high HER2-specific uptake in SKOV-3 cells, achieving >99% internalization within 1 h, consistent with findings reported by Gaweda et al. (143, 144). The authors compared the cytotoxicity of radiobioconjugates labeled with the Auger emitter ^{125}I ($t_{1/2} = 59.49$ d; Au@Pd ^{125}I -trastuzumab), β^- emitter ¹⁹⁸Au (t_{1/2} = 2.69 d; ¹⁹⁸Au-trastuzumab), and the ¹⁰⁹Pd/^{109m}Ag in vivo generator (Au@¹⁰⁹Pd-trastuzumab) (143). With consistent activity concentrations of 20 MBq/ml, the ¹⁰⁹Pd/^{109m}Ag-based conjugate demonstrated significantly higher cytotoxicity than those conjugates radiolabeled with either 125I or ¹⁹⁸Au, highlighting the therapeutic advantage of simultaneous emission of both radiation types from this generator design (143). A subsequent study in 2024 (145) improved ¹⁰⁹Pd production using 108Pd, achieving >500 MBq/mg from the natural palladium target and >2 GBq/mg from the enriched palladium target (78). Their findings indicated that Pd NPs labeled with 109Pd were significantly more cytotoxic at similar activities than those labeled with either 131 or 125 (145). Analogous to 103Pd, Annamalaisamy et al. (115) also reported the radiosynthesis and evaluation of 109Pd/109mAg in situ generator bound to a mixed bipyridyl-bisphosphonate scaffold, ¹⁰⁹Pd₂(bpy)₂ale, for bone-targeted radionuclide therapy. in vitro, the conjugate significantly reduced metabolic viability in prostate and ovarian cancer cells, with cytotoxicity depending on both activity concentration and exposure time (115).

4 Osmium and osmium-based radionuclide

Naturally occurring osmium consists of seven stable isotopes: $^{184}\mathrm{Os}$ (0.02%), $^{186}\mathrm{Os}$ (1.59%), $^{187}\mathrm{Os}$ (1.97%), $^{188}\mathrm{Os}$ (13.24%), $^{189}\mathrm{Os}$ (16.15%), $^{190}\mathrm{Os}$ (26.26%), and $^{192}\mathrm{Os}$ (40.78%) (19). Radioisotopes include $^{185}\mathrm{Os}$, $^{191}\mathrm{Os}$, $^{193}\mathrm{Os}$, and $^{194}\mathrm{Os}$, in this review we will only discuss $^{191}\mathrm{Os}$.

4.1 Osmium-191, ¹⁹¹Os

¹⁹¹Os ($t_{1/2}$ = 15.4 d) decays to ^{191m}Ir ($t_{1/2}$ = 4.96 s) by β⁻ emission (100%), suitable for an ¹⁹¹Os/^{191m}Ir generator used for first-pass radionuclide angiocardiography (146). Cheng et al. (147) first used ¹⁹¹Os in the development of the ¹⁹¹Os/^{191m}Ir generator (148). The long half-life facilitates its use in generator construction, quality-control, and clinical use distant from production facilities (146, 149).

4.1.1 Production and radiochemical separation of ¹⁹¹Os

Shown in Table 3, Salek et al. (149) irradiated isotopically enriched osmium (190 Os, 97.8%) in the 5 MW Tehran Research Reactor ($\phi = 4 \times 10^{13}$ n cm $^{-2}$ s $^{-1}$) for 15 days with subsequent fusion in a mixture of KOH-KNO₃, reporting a specific activity of \sim 325 mCi/mg. The dissolution method for osmium reported by Brihaye et al. (150) has been established in subsequent steps

to form K2OsCl6; and carried out for all reported studies in this review. Additionally, osmium by-products 185 Os ($t_{1/2} = 15.4$ d) via 184 Os(n, γ) 185 Os reaction and 193 Os ($t_{1/2} = 30.2 \text{ h}$) via $^{192}\text{Os}(n,\!\gamma)^{193}\text{Os}$ reaction are produced only in trace amounts (149). These are neglected as ¹⁸⁵Os decays to stable ¹⁸⁵Re, and ¹⁹³Os decays quickly (149). However, an unavoidable longerlived impurity is 192 Ir ($t_{1/2} = 73.8$ d), which is produced when stable 191 Ir—the stable decay product of 191 Os—undergoes a 191 Ir(n, γ) 192 Ir reaction during irradiation (146, 149, 151). Brihaye et al. (150) demonstrated two separation methods distillation and solvent extraction—between 191Os and 192Ir. Using these methods, they achieved a separation efficiency of 100% by distillation and 99.9% efficiency by solvent extraction (150). Salek et al. (149) modified the extraction method and yielded a $98.8 \pm 0.48\%$ ¹⁹¹Os recovery, while completing the procedure in 30 min.

4.1.2 Applications of ¹⁹¹Os

In a study performed by Jamre et al. (148), BLM (Figure 6A) was radiolabeled with 191 Os by reacting it with K_2 OsCl₆. The total labeling and formulation of 191 Os-BLM took approximately 24 h, resulting a >95% radiochemical yield and >97% radiochemical purity, with <3% free 191 Os- K_2 OsCl₆ detected by radio-TLC (148). They reported the 191 Os-BLM complex remained stable in aqueous solution for \sim 72 h. Biodistribution studies (4 h, 24 h, 48 h, 72 h, and 14d p.i.) for 191 Os-BLM demonstrated high uptake in the lungs and moderate accumulation in the liver and spleen, all remaining >1% ID/g throughout the study (148). *In vivo* imaging at 24, 48, and 72 h confirmed these retention patterns as well (148).

TABLE 3 Production route for ¹⁹¹Os.

Radionuclide	Nuclear reaction	Flux/Energy	References
¹⁹¹ Os	$^{190}{\rm Os}(n,\gamma)^{191}{\rm Os}$	$4 \times 10^{13} \text{ n cm}^{-2}$ s^{-1}	(149)

Labeling APMTS (Figure 6B) with 191Os, Moghaddam et al. (152) achieved >95% radiochemical yield in a 12 h synthesis with a specific activity of 21.5 GBq/mmol, while the complex remained >95% stable for at least 48 h (152). In the biodistribution studies (4, 24, 48, and 72 h p.i.) using the ¹⁹¹Os-APMTS complex, liver uptake and kidney uptake peaked by 48 h (5.2%-6.7% ID/g), while there was low blood, heart, bone retention by 24 h and negligible by 72 h (<0.5% ID/g) (152). A follow-up study by Moghaddam-Banaem et al. (151), demonstrated the preparation of 191Os-phyate complex shown in Figure 6C that could be used for radiosynovectomy applications. Using 10 mg of sodium phytate, the complex forms in ~24 h with a labeling yield >98% detected by radio-chromatography, while remaining stable in an aqueous solution for at least 72 h (151). Biodistribution studies (0.5, 4, 24, 72 h p.i.) showed most of the injected dose remained in the joint with minimal uptake in the kidney, and other organs considered negligible (<0.5% ID/g) (151).

5 Iridium and iridium-based radionuclide

Iridium has two naturally occurring stable isotopes, ¹⁹¹Ir (37.3%) and ¹⁹³Ir (62.7%) (19). Radioisotopes include ^{191m}Ir, ^{192m}Ir. In this review we will only discuss ¹⁹²Ir.

5.1 lridium-192, ¹⁹²lr

The radionuclide 192 Ir ($t_{1/2}$ = 78.83 d) is an important therapeutic radionuclide, particularly in brachytherapy, due to the favorable nuclear properties including 95% β^- emission ($E_{\beta-}$ = 7 MeV) and 5% electron capture (153). Furthermore, two notable γ -ray energies include 316 keV (I_{γ} = 82.7%) and 468 keV (I_{γ} = 47.8%) (153). Bertermann and Brix (154) obtained preliminary results for the use of 192 Ir in high dose rate (HDR) brachytherapy to treat prostate cancer (155, 156).

FIGURE 6

(A) Bleomycins (BLMs) are tumor seeking antibiotics that have been widely used in cancer chemotherapy, where these compounds are activated by cation insertion as anti-neoplastic agents; therefore, resulting in DNA decomposition (148). (B) Moghaddam et al. (152) labeled 2-acetyl pyridine 4-N-methylthiosemicarbazone (APMTS) with ¹⁹¹Os (elemental Os shown in structure) to develop a potential *in vivo* tumor-targeting radionuclide generator. (C) Moghaddam-Banaem et al. (151) labeled the salt form of phytic acid, phytate, and radiolabeled with ¹⁹¹Os (¹⁹¹Os-phytate) to develop an *in vivo* radionuclide generator.

5.1.1 Production and radiochemical separation of ¹⁹²Ir

Due to its widespread use, 192 Ir is routinely produced in nuclear reactors via the 191 Ir(n, γ) 192 Ir reaction, using either Na₂IrCl₆ targets —described by Ananthakrishnan (157)—or iridium wire, as applied in clinical settings by Schaeken et al. (153, 158). All production routes are shown in Table 4. Irradiating Na₂IrCl₆ under standard conditions —10 mg; $\phi = 1.5 \times 10^{13}$ n cm⁻² s⁻¹; 7 days—can yield 12 GBq of 192 Ir, with specific activity >185 GBq per gram Ir (157). After irradiation, the targets are dissolved in 10 ml of 0.1 N HCl, yielding radiochemical solutions with concentrations ranging from 74 to 370 MBq/ml and >99% radionuclidic purity (157). This method remains the benchmark for high-activity, high-purity 192 Ir production for clinical brachytherapy (157). As reactor-produced 192 Ir is carrier-added, accelerator routes have been explored to produce n.c.a. 192 Ir with potentially higher specific activity.

Via the ¹⁹²Os(p,n)¹⁹²Ir reaction, Hilgers et al. (153) measured a peak cross-section of 68 ± 8 mb at 9.1 ± 0.5 MeV, while identifying an optimal production window of 8-16 MeV $(\sim 0.16 \text{ MBq/}\mu\text{A-h})^{192}\text{Ir}$. The authors confirmed their experimental data with nuclear model codes [EMPIRE-II (96) and ALICE-IPPE (159)] and pointed out that though a cyclotron approach yields lower activity than those achieve via reactor-based production, the specific activity could be much higher (153). They estimated under realistic irradiation conditions (30 h, $\phi = 3.74 \times 10^{15}$ p/s), projected batch yields could reach ~5.6 GBq—serving as a complementary approach and broadening access to high specific activity 192 Ir brachytherapy sources (153). Langille et al. (155) demonstrated that a 12.8 MeV proton beam on naturally abundant, electroplated osmium targets yields 192 Ir with an average measured cross section of 46.4 ± 6.2 mb, which compared well with literature values of Hilgers et al. (153) and Szelecsenyi et al. (160). Targets underwent oxidative dissolution (H2O2/HCl) and anion-exchange chromatography on Dowex 1×8 , with the process delivering an overall radiochemical efficiency of ~80% and radionuclidic purity of 100% (155). Building on established microwave-assisted syntheses of non-radioactive complexes [(ppy)₂Ir(μ-Cl)₂Ir(ppy)₂] and Ir(ppy)₂(bpy)—reported earlier by Alam et al. (161), Bura et al. (162), and Wu et al. (163)—the authors performed the first radiosynthesis of an iridium cyclometallation reaction by adding n.c.a. [IrCl₆]³⁻ to the microwave reaction (155). They achieved up to 68% radiochemical purity of Ir(ppy)₂(bpy) with a maximum specific activity of 0.54 ± 0.14 Ci μ mol⁻¹ (20 ± 5.2 GBq μ mol⁻¹) (155).

TABLE 4 Production routes for ¹⁹²Ir.

Radionuclide	Nuclear reaction	Flux/Energy	References
¹⁹² Ir	¹⁹¹ Ir(n,γ) ¹⁹² Ir	$1-1.5 \times 10^{13} \text{ n cm}^{-2}$ s^{-1}	(157, 158)
	¹⁹² Os(p,n) ¹⁹² Ir	19 → 6 MeV	(153, 155, 160)
	¹⁹² Os(d,2n) ¹⁹² Ir	21 → 5 MeV	(164)
	193 Ir(γ ,n) 192 Ir	$E_{\text{max}} = 40 \text{ MeV}$	(165)

Tarkanyi et al. (164) reported the first experimental cross sections for the ¹⁹²Os(d,2n)¹⁹²Ir reactions up to 21 MeV, employing a stacked-foil technique with 84.5% enriched ¹⁹²Os targets electrodeposited on 25 µm thick Ni foils, thereby observing a cross sectional peak of 370 ± 46 mb at 12.1 ± 0.8 MeV. Although reactor-based ¹⁹²Ir production yields remain higher, the deuteron route results in a n.c.a. product of ¹⁹²Ir with significantly higher specific activity (153, 164). Compared with the earlier ¹⁹²Os(p,n) process via Hilgers et al. (153), the (d,2n) channel delivers higher cross sections and thick-target yields in the same energy window; however, due to smaller and higher-current proton cyclotrons being more readily available, the choice for the $^{192}\mathrm{Os}(p,\!n)\text{-reaction}$ is preferred (164). Dovbnya et al. (165) reported the first experimental demonstration of photonuclear 193 Ir $(\gamma,n)^{192}$ Ir on natural iridium using a tantalum bremsstrahlung converter integrated within a neutron moderator, which enhanced 192 Ir yields by ~50% via the 191 Ir $(n,\gamma)^{192}$ Ir reaction and delivered up to ~900 MBq/h under 40 MeV, 4 µA beam conditions. Computational simulations with PENELOPE-2008 software (166) supplemented by evaluated photonuclear cross sections accurately reproduced experimental yields for 192Ir as well as coproduces isotopes (190 Ir, 90 Mo, 99 Mo), validating the mixed γand n-flux model (165). Compared to traditional reactor-based 191 Ir(n, γ) 192 Ir production (74 MBq/h; >1,000 MBq/h-g) and cyclotron-based ¹⁹²Os(p,n)¹⁹²Ir production (>185 MBq/h; without carrier), this electron-accelerator approach offers competitive batch yields and modular flexibility (153, 157, 165). While the specific activity is low, the authors suggest that optimizing activation-cooling regimes and employing enriched ¹⁹³Ir targets could enable scalable, reactor-free ¹⁹²Ir production suitable for medical and industrial applications (165).

5.1.2 Applications of ¹⁹²Ir

brachytherapy, offering a steep dose gradient that concentrates therapeutic radiation within tumors while minimizing damage to the surrounding normal tissue (167). Jayakody et al. (167) reviewed a suite of independent verification methods—including radiochromic films, ionization-chamber arrays, plastic scintillation detectors, and TLD/OSLD systems—that have been benchmarked against TPS-calculated dose maps for ¹⁹²Ir. Roussakis and Anagnostopoulos (168) wrote a mini-review on the aspects of the Iridium-Knife, detailing the key physical properties of the ¹⁹²Ir HDR source and illustrating how these underlie its characteristic steep dose gradients.

Nohara et al. (169) reported that 166 localized prostate cancer patients treated with a 44 Gy EBRT and 3×6 Gy 192 Ir HDR boost achieved a 5-year biochemical recurrence-free survival of 93.0%. Shigehara et al. (170) observed a 4-year overall survival of 87.2% and PSA progression-free survival of 82.6% in 84 prostate patients receiving 18 Gy 192 Ir HDR and 44 Gy EBRT. Chin et al. (171) treated 65 prostate cancer patients with EBRT plus two 8.5 Gy 192 Ir HDR fractions, reporting a 3-year biochemical disease-free rate of 90.8%. Potter et al. (172) used CT-planned 192 Ir HDR and 48.6–50 Gy EBRT in 189 cervical cancer patients,

achieving 3-year pelvic control of 77.6% and disease-specific survival of 68.6%. Ott et al. (173) demonstrated that interstitial ¹⁹²Ir accelerated partial breast irradiation (APBI) in 69 early-stage breast cancer patients which yielded 100% 2-year local control, minimal acute and late toxicity, in 90% of cases.

Abtahi et al. (174) conducted a systematic review (1984-2020) between 192Ir and 60Co in GYN cancers. They reported that the 5-year overall survival (OS), local control, disease-free survival (DFS) and high-grade GI/GU toxicity were statistically equivalent between the two (174). Wen et al. (175) compared miniaturized HDR sources for cervical brachytherapy and found nearly identical dose distributions within 25 mm of the source, with equivalent clinical outcomes and toxicity rates. Strohmaier and Zwierzchowski (176) reviewed the physical and logistical aspects of 60Co vs. 192Ir, concluding that the two radionuclides matched in radial dose function, while delivering equivalent clinical efficacy. Tantivantana and Rongsriyam (177) performed a retrospective analysis of 480 stage IB2-IIIB cervical cancer patients treated between 2004 and 2014, comparing outcomes following HDR brachytherapy with 192 Ir (274 patients; 57.1%) or ⁶⁰Co sources (206 patients; 42.9%). The study found no statistically significant differences in OS, recurrence rate, or DFS between the ¹⁹²Ir and ⁶⁰Co cohorts (177).

6 Rhodium and Rhodium-based radionuclides

Rhodium has one naturally occurring stable isotope, 103 Rh (100%) (19). Radioisotopes include 99 Rh, 101 Rh, 101m Rh, 102m Rh, 103m Rh, and 105 Rh, in this review we will only discuss 103m Rh and 105 Rh.

6.1 Rhodium-103 m, 103mRh

An isomer of rhodium that has seen applications in targeted radionuclide therapy due to its Auger electrons is $^{103\mathrm{m}}\mathrm{Rh}$ (t_{1/2} = 56.1 min). It has also been involved in convenient generator pairs with $^{103}\mathrm{Pd}$ and $^{103}\mathrm{Ru}$, respectively, *in vivo* (118, 178).

6.1.1 Production and radiochemical separation of ^{103m}Rh

The production for 103m Rh is shown in Table 5. Epperson et al. (179) introduced a rapid, high-yield generator for 103m Rh by solvent-solvent extraction of RuO₄ into CCl₄ achieving $94 \pm 0.6\%$ 103m Rh yield with $3.8 \pm 0.7\%$ 103 Ru contamination in a single, 15-min extraction. This method contrasts with earlier ion-exchange and distillation approaches referenced by the authors, offering a practical foundation for routine on-demand 103m Rh availability (179). Bartos et al. (178) similarly used reactor-produced 103 Ru (from natural ruthenium irradiation of 36 h, yielding 466 MBq) and separated 103m Rh from RuO₄ extraction. This work laid the foundation for supplying shortlived 103m Rh in sufficient quantities for further studies (178). Thery et al. (180) reported the recent progress in ruthenium

TABLE 5 Production routes for rhodium-based radionuclides.

Radionuclide	Nuclear reaction	Flux/Energy	References
^{103m} Rh	102 Ru(n, γ) 103 Ru \rightarrow 103m Rh	$3 \times 10^{14} \text{ n cm}^{-2} \text{ s}^{-1}$	(178, 179, 184)
	$\begin{array}{c} ^{102}\text{Pd}(\text{n},\!\gamma)^{103}\text{Pd} \rightarrow \\ ^{103\text{m}}\text{Rh} \end{array}$	$1.2-1.4 \times 10^{15} \text{ n}$ $\text{cm}^{-2} \text{ s}^{-1}$	(118, 181, 184)
	103 Rh(p,n) 103 Pd \rightarrow 103m Rh	Ep = 14–18 MeV	(118, 181, 184)
¹⁰⁵ Rh	104 Ru(n, γ) 105 Ru \rightarrow 105 Rh	$3-8 \times 10^{13} \text{ n cm}^{-2}$ s^{-1}	(188, 191)
	$^{106}\text{Pd}(\gamma,p)^{105}\text{Ru} \rightarrow ^{105}\text{Rh}$	$E_{\text{max}} = 55 \text{ MeV}$	(195, 197)
	natPd(p,x)105Rh	40 → 4 MeV	(198)

chemistry for the ¹⁰³Ru/^{103m}Rh generator for Auger therapy, describing the main limiting factor being an effective separation between the two radionuclides due to the unpredictable, misunderstood chemistry. Their work overcame prior barriers in earlier solvent-extraction and speciation studies, establishing optimal conditions for examining the experimental feasibility of the generator in the future (180).

More recently, Jensen et al. (118) demonstrated a solid-phase ¹⁰³Pd/^{103m}Rh generator using neutron-activated ¹⁰²Pd targets. They chelated carrier-added ¹⁰³Pd with a lipophilic macrocycle, 16aneS4, and loaded it on a C18 cartridge (118). The optimal elution performance for 103mRh was achieved with 1.0 M HCl, yielding a radiochemical purity of 99%, an apparent molar activity of 26.6 MBq/nmol, and an elution yield of 5.81% (118). Despite the potential, the low elution yield indicates that further optimization is necessary to utilize the generator for extended use, particularly in clinical applications (118). Ohya et al. (181) improved on this by testing various anion-exchange resinsinspired by Berk (182) and Mamadaliev et al. (183)-following a separation method described in Ohya et al. (101). Four commercially available gel-type anion-exchange resins with comparable functions groups and matrixes were investigated: IRA410 and SA20A (dimethylethanol ammonium), and IRA904 and SA11AL (trimethyl ammonium) (181). Of these, SA11AL delivered the best performance, with a raw yield of 39% and lowest 103Pd breakthrough of 0.29% over 32 milking cycles spanning eight weeks (181). More recently, Zagryadsky et al. (184) performed measurements of the ¹⁰²Pd(n,y)¹⁰³Pd and ¹⁰²Ru $(n,\gamma)^{103}$ Ru reactions in the IR-8 Reactor for the purpose of ¹⁰³Ru/^{103m}Rh and ¹⁰³Pd/^{103m}Rh generators. They indicated the experimental channel of the IR-8 reactor will be capable of achieving sufficiently 103Ru and 103Pd for the utilization of ^{103m}Rh in radiopharmaceuticals (184).

6.1.2 Applications of ^{103m}Rh

Bernhardt et al. (185) performed Monte Carlo simulations to model the metastatic growth of tumor sizes for radionuclide therapy, comparing between high-energy electron emitter 90 Y ($t_{1/2} = 64.05$ h), medium-energy electron emitter 177 Lu ($t_{1/2} = 6.65$ d), and the low-energy electron emitter $^{103\text{m}}$ Rh. They observed for low tumor-to-normal (TNC) tissue activity

concentrations, 103m Rh performed slightly better compared to 177 Lu; however, for high TNC values, 103m Rh was the best choice for tumor treatment (185). However, as the authors noted, the short half-life ($t_{1/2}$ = 56.1 min) may be a limitation in the adaptation as an optimal radiotherapeutic (185).

6.2 Rhodium-105, 105Rh

¹⁰⁵Rh ($t_{1/2}$ = 35.36 h) is an attractive candidate for radiotherapeutic applications due to its nuclear characteristics (186). ¹⁰⁵Rh decays via β⁻-emission with energies of 179 keV (75.0%), 74 keV (5.2%), and 70 keV (19.7%), along with two low-abundant γ-rays at 319 keV ($I_γ$ = 20%) and 306 keV ($I_γ$ = 5%) —useful for mapping the *in vivo* uptake of the administrator radiopharmaceutical (78, 187, 188). Grazman and Troutner (189) first explored the viability of ¹⁰⁵Rh and its properties for use as a radiotherapeutic agent (190).

6.2.1 Production and radiochemical separation of ¹⁰⁵Rh

Described in Table 5, Jia et al. (191) developed a scalable route to n.c.a. ¹⁰⁵Rh by irradiating enriched ¹⁰⁴Ru in the MURR reactor $(\phi = 8 \times 10^{13} \text{ n cm}^{-2} \text{ s}^{-1}, 72 \text{ h})$, achieving average yields of $\sim 5 \text{ mCi}$ per mg Ru and >85% total recovery of 105Rh. Their MgO adsorption method eliminated the need for chlorine gas and the formation of RuO₄—required in an earlier approach (189) while delivering a ruthenium decontamination factor of 16,600, supporting the reliable availability of 105Rh in large quantities (191). Subsequently, Unni et al. (188) developed a methodology for the production and purification of carrier-free ¹⁰⁵Rh by irradiating natural Ru (99.9%) at a thermal flux of 3×10^{13} n cm⁻² s⁻¹ for 5-7 days, followed by a 24 h decay of 105 Ru to 105 Rh, achieving within 5% of \approx 24 mCi predicted by Bateman's equation. The authors oxidized the Ru matrix (97Ru, ¹⁰³Ru, and trace ¹⁹²Ir) to volatile RuO₄ (KIO₄/KOH at 70°C, 20 min), performed successive solvent extractions with CCl₄ (retaining $97.8 \pm 0.78\%$ of 105 Rh in aqueous phase), and then applied 100% TBP extraction to obtain $95.35 \pm 0.78\%$ of ^{105}Rh (aqueous phase) and $96.6 \pm 0.8\%$ of ¹⁹²Ir (organic phase) (188). A co-precipitation of 105Rh with Fe(III) as hydroxide using KOH recovered $89.4 \pm 2.2\%$ of 105 Rh, and a three-stage Fe removal—using cationic exchange chromatography—delivered a final overall recovery of ~80% (15-20 mCi) of carrier-free ¹⁰⁵Rh (188). Okoye et al. (192) demonstrated a comprehensive strategy to reclaim, purify, and reuse enriched 104Ru targets—originally captured as RuO₄ in 3 M HCl from decades of ¹⁰⁵Rh production -for economical, high-yield 105Rh manufacture. The recycled metal retained 98.84% 104Ru enrichment—a slight decrease from their original—and enabled up to 97.3% 105Rh recovery (19.10 mCi) (192). The isolated 105Rh was subsequently used in radiolabeling experiments with two previously developed chelators (193, 194), yielding radiochemical efficiencies of $91.0\% \pm 1.5$ for $222-S_4$ -diAcOH (Figure 7A) and $80.9\% \pm 0.4$ for 16S₄-diol (Figure 7B) (192).

Inagaki et al. (195) investigated the production of 105Rh via two distinct routes: neutron irradiation of natRuO4 powder $(\phi = 4.5 \times 10^{12} \text{ n cm}^{-2} \text{ s}^{-1}, 10 \text{ min}) \text{ through the } ^{104}\text{Ru}(n,\gamma)^{105}\text{Ru}$ reaction; and bremsstrahlung photon irradiation of natural Pd foils (5 × 5 mm²) at 20-40 MeV using an electron linear accelerator (linac), inducing the $^{106}Pd(\gamma,p)^{105}Ru$ reaction. To enable comparison, the authors normalized yield data to equivalent target masses, beam currents, and irradiation times, reporting 77 ± 2 kBq of ¹⁰⁵Rh via the reactor method (10 mg) and 88 ± 5 kBq at 40 MeV from the linac method (50 mg, 100 μA, 10 min) (195). Furthermore, extrapolation to clinicalscale conditions using the linac method-10 g Pd target, 1 mA current, and 24 h irradiation—predicted a 105Rh yield of approximately 20.1 GBq, far exceeding the 0.148 GBq typically required for diagnostic or therapeutic applications, as described in Sciuto et al. (195, 196). Kazakov et al. (197) investigated a method for producing carrier-free 105Rh using a 55 MeV electron accelerator, analyzing the isotopic composition of irradiated PdCl2 and optimizing separation methods. Irradiation of 270 mg PdCl₂ in 5 ml solution at 100 nA for 1 h yielded 73.7 kBq/µAh of total rhodium activity, with ¹⁰⁵Rh containing 82% (60 kBq/µAh, 2.1 kBq (197). When compared to Inagaki et al. (195), who reported 88 kBq from 50 mg natPd foil for at 40 MeV (10 min, 100 nA), both demonstrated feasible accelerator-based alternatives to reactor or cyclotron production for medical applications (197). Nonetheless, the irradiated PdCl₂ was dissolved in 2 M HCl and passed through extraction chromatography columns using either DGA-Normal or TEVA resins (197). Column and distribution coefficient studies showed DGA-Normal offered superior performance, eluting ≥98% of ¹⁰⁵Rh in 2 M HCl and enabling complete Pd stripping with 11 M HCl (Pd/Rh separation factor >10⁵), while TEVA failed to achieve sufficient Pd/Rh separation (197).

Khandaker et al. (198) reported the first experimental measurement of $^{\rm nat}{\rm Pd}({\rm p,x})^{105}{\rm Rh}$ excitation function from 4 to 40 MeV using stacked-foil activation, observing significant discrepancies between measured cross-sections and nuclear model predictions from TALYS (49) and ALICE-IPPE (159). From the experimental data, thick target yield calculations suggest that low-energy cyclotrons (E < 20 MeV) can effectively produce $^{105}{\rm Rh}$, primarily via the $^{108}{\rm Pd}({\rm p,\alpha})^{105}{\rm Rh}$ reaction (198).

6.2.2 Applications of ¹⁰⁵Rh

Jurisson et al. (187) investigated ¹⁰⁵Rh radiopharmaceutical development by exploring a suite of cis- and trans-[RhCl₂l]⁺ complexes using tetradentate thioether ligands. Brooks et al. (190) reported the synthesis and purification of novel ¹⁰⁵Rh-bleomycin (¹⁰⁵Rh-BLM) complex, demonstrating >80% complexation yield, high *in vitro* stability, and rapid biphasic *in vivo* clearance with minimal non-specific retention. Although ¹⁰⁵Rh-BLM achieved tumor uptake approximately four-fold greater than contralateral muscle, its potential for targeted radiotherapy is limited by significant levels and prolonged retention in the kidneys relative to tumor (190). The study by Ando et al. (199) evaluated ¹⁰⁵Rh as a candidate for radiotherapeutic applications targeting bone metastases by

FIGURE 7

Okoye et al. (192) labeled 105 Rh successfully with previously used chelators for Rh(III) complexation, (A) the tetrathioether ligand (222-S₄-diAcOH) by Goswami et al. (193) and (B) the tetradentate thiamacrocyclic ligand (16S₄-diol) by Venkatesh et al. (207). (C) In an early study by Ando et al. (259), 177 Lu can be chelated to ethylenediamine-tetra-methylene phosphonic acid, EDTMP, producing a bone-seeking phosphonate complex that is chemical and biologically stable. Therefore, the same group (199) investigated the biological behavior of 105 Rh when chelated to EDTMP.

leveraging its favorable decay properties and investigating its biological behavior when chelated to EDTMP shown in Figure 7C. Radiolabeling with EDTMP achieved >99% labeling efficiency, with no dissociation observed for up to 5 days at room temperature (199). Compared to a study using ^{99m}Tc-MDP by Sanada et al. (200), ¹⁰⁵Rh-EDTMP demonstrated comparable bone uptake, but exhibited faster clearance from circulation and significantly higher bone-to-tissue ratios (199). Mentioned in Okoye et al. (192), a variety of chelates have been evaluated (186, 193, 194, 201–213), along with preclinical biological distribution studies have been highlighted in Li et al. (209) and Goswami et al. (193) for ¹⁰⁵Rh clinical utility towards advancing therapeutic radiopharmaceuticals.

7 Ruthenium and ruthenium-based radionuclides

Ruthenium has seven naturally occurring isotopes: ⁹⁶Ru (5.6%), ⁹⁸Ru (1.87%), ⁹⁹Ru (12.76%), ¹⁰⁰Ru (12.6%), ¹⁰¹Ru (17.06%), ¹⁰²Ru (31.55%), and ¹⁰⁴Ru (18.62%) (19). Radioisotopes of ruthenium include ⁹⁷Ru, ¹⁰³Ru, and ¹⁰⁶Ru, where our review will focus on ⁹⁷Ru and ¹⁰³Ru. ¹⁰⁶Ru, which has been predominantly involved in brachytherapy in the last 25 years (4, 214–227), was omitted in this review, due to lack of applications in nuclear medicine.

7.1 Ruthenium-97, 97Ru

 97 Ru (t_{1/2} = 2.8 d) decays by electron capture (100%) to 97 Rh, with the emission of low-energy γ -rays, 216 keV (86%) and 324 keV (11%) (228). This radionuclide provides excellent conditions for *in vivo* imaging, as it is within the energy window of clinical SPECT detectors (228).

7.1.1 Production and radiochemical separation of $^{97}\mbox{Ru}$

The production routes for ⁹⁷Ru are listed in Table 6. Zaitseva et al. (229) measured excitation functions for ⁹⁷Ru production via

the ⁹⁹Tc(p,3n)⁹⁷Ru reaction, using a stacked-foil technique (50-100 nA) from 20 to 99 MeV. They measured a 438 ± 66 mb peak at 32 MeV-corresponding to a thin-target yield of ~934 μCi/ μAh —and a cumulative yield of $\sim 10.49 \text{ mCi/}\mu Ah$ when degrading protons from 99 MeV to the threshold $(E_{th} = 18.3 \text{ MeV})$ (229). An optimal 19–50 MeV window maximized ⁹⁷Ru production (~7 mCi/μAh) while higher-energy beams (>50 MeV) could push yields beyond 10.5 mCi/µAh for Ci-scale production at higher currents (229). Building on this, Zaitseva et al. (230) optimized a radiochemical separation for metallic Tc targets irradiated at 50 MeV (~8 μA, 1 h), isolating 40-50 mCi of 97Ru. A four-step process—dissolution, acid conversion, oxidation-distillation, and absorption-reduced Ru (VIII) to Ru(III) and recovered 95%-98% of Ru with >10⁴ purity after 6-7 h (230). An estimated delivery of ≥150 mCi of ⁹⁷Ru is needed (50 MeV, 6–8 μA, 8 h) for clinical purposes to be feasible ~70 h after EOB (230).

Ditroi et al. (231) and Tarkanyi et al. (232) explored α -induced routes on natural molybdenum, measuring 97Ru excitation functions up to 40 MeV. Both found peaks near 39 MeV $(182.4 \pm 20.5 \text{ mb})$ and $232 \pm 26 \text{ mb}$, respectively), along with good agreement from previous results by Levkovskij (233) and Graf and Munzel (234) across all energy ranges, and with Rapp et al. (235) at low energies (231, 232). Model comparisons (TENDL-2011/TENDL-2015 (49), ALICE-IPPE (159), and EMPIRE-3.1 (96)) generally agreed in trend, with (232) calculating thicktarget yields reaching 2 GBq/C (0.19 mCi/µAh), and potential to increase the yield by a factor of three through isotopic enrichment favoring the $^{94}\text{Mo}(\alpha,n)$, $^{95}\text{Mo}(\alpha,2n)$, and $^{96}\text{Mo}(\alpha,3n)$ reactions. Thick target yields were described by Abe et al. (236), thereby obtaining a yield of 126 μCi/μAh via the ⁹⁴Mo(α,n) reaction using 30 MeV α-particles (232). Sitarz et al. (237) extended α-induced production of ⁹⁷Ru to 67 MeV, confirming a 237 ± 20 mb at 41.8 MeV, agreeing with (232) and (231) below 40 MeV. Most recently, Happl et al. (238) demonstrated 97Ru production for α-induced irradiation of ^{nat}Mo for 10 h to yield >300 MBq end of irradiation (EOI). Post-irradiation, the target foil was dissolved and bulk Mo was removed using two sequential ion exchange columns; obtaining trace impurities of Mo (0.9-2.0 μg) and minor radionuclidic contaminants

TABLE 6 Production routes for ruthenium-based radionuclides.

Radionuclide	Nuclear reaction	Flux/Energy	References
⁹⁷ Ru	⁹⁹ Tc(p,3n) ⁹⁷ Ru	E _{max} = 99 MeV	(229, 230)
	$^{\mathrm{nat}}\mathrm{Mo}(\alpha,n)^{97}\mathrm{Ru}$	$E_{max} = 67 \text{ MeV}$	(231, 232, 237, 238)
	$^{89}\text{Y}(^{12}\text{C},4\text{n})^{97,97\text{m}}\text{Rh} \rightarrow ^{97}\text{Ru}$	70 → 65 MeV	(239)
	⁸⁹ Y(¹² C,p3n) ⁹⁷ Ru	70 → 65 MeV	(239)
¹⁰³ Ru	$^{\mathrm{nat}}\mathrm{Mo}(\alpha,n)^{103}\mathrm{Ru}$	$40 \rightarrow 8 \text{ MeV}$	(231, 232)
	²³² Th(p,f) ¹⁰³ Ru	$E_{\text{max}} = 89.6 \text{ MeV}$	(245)
	$^{\mathrm{nat}}\mathrm{Ru}(\mathrm{n},\gamma)^{103}\mathrm{Ru}$	$5-10 \times 10^{14} \text{ n cm}^{-2} \text{ s}^{-1}$	(238, 243, 246)

including 95 Ru (t_{1/2} = 1.6 h), 95m Tc (t_{1/2} = 61.0 h), and 95 Tc (t_{1/2} = 20.0 h) in the 97 Ru eluate (238). The reported radiochemical yield of 97 Ru was 40%–56%, resulting in deliverable activities of 87–123 MBq (74–106 MBq/ml) (238).

Furthermore, Maiti and Lahiri (239) introduced a novel $^{12}\text{C} + ^{89}\text{Y}$ production route for n.c.a ^{97}Ru , while avoiding coproduction of longer-lived radionuclides to achieve tracer-level yields after cooling. Furthermore, the authors developed a two-separation scheme—a solid-liquid extraction in 1 M HCl and sequential 0.1 M/6 M HCl column chromatography—yielding 88% n.c.a. ^{97}Ru and resulting distinct Ru(IV)/Ru(III) speciation under certain conditions (239).

7.1.2 Applications of ⁹⁷Ru

Oster et al. (240) evaluated ⁹⁷Ru-DTPA as a potential imaging agent for cerebrospinal fluid by injecting 0.4 mCi of the compound into the cisterna magna of dogs, while comparing the performance with ¹¹¹In-DTPA. From their study, they established 97Ru-DTPA to be superior to 111In-DTPA as it delivered approximately half the absorbed dose to the tissues, along with better imaging capabilities (240). Som et al. (241) labeled transferrin with 97Ru (97Ru-TF) and compared its biodistribution to ⁶⁷Ga-citrate, ¹²³I-transferrin, ^{99m}Tc-plasmin, ¹²⁵I-fibrinogen, and ¹³¹I-albumin in tumor and abscess bearing animals. Notably, the difference between 97Ru-TF and 67Gacitrate were of particular focus, as tumor concentrations of ⁹⁷Ru-TF increased substantially with time, whereas the ⁶⁷Ga concentration did not (241). The authors noted although there were no significant advantages using ⁹⁷Ru over ⁶⁷Ga, the nuclear characteristics of ⁹⁷Ru may improve imaging quality (241).

More recently, as a potential radiopharmaceutical, Borisova et al. (242) reported the first ⁹⁷Ru complex with pyridine-2,6-dicarboxamide conjugate shown in Figure 8A (243). Happl et al. (238) further explored the same method from Happl et al. (243) for a three-step synthesis for radiolabeling BOLD-100 (Figure 8B) with c.a. [⁹⁷Ru]RuCl₃ (0.2–0.5 MBq/μmol). The radiochemical purity of all three intermediates was >99% (238). The final product exhibited an overall radiochemical yield of 8% and an overall chemical yield of 13%, based on the mass of isolated intermediates and products (238). Additionally, the specific activity at the end of synthesis was 0.1 MBq/mg, with a molar activity of 0.05 MBq/μmol (238). Although radiolabeling BOLD-100 with ⁹⁷Ru was successful, the radiochemical yield and specific activity must be improved to enable SPECT imaging using c.a. [⁹⁷Ru]BOLD-100 (238).

7.2 Ruthenium-103, 103 Ru

¹⁰³Ru (t_{1/2} = 39.3 d) decays by β⁻-emission (100%), and has two γ -rays, 497 keV (91%) and 610 keV (6%) (238). Although this radionuclide has therapeutic applications, its use in the ¹⁰³Ru/^{103m}Rh generator is of importance as well.

7.2.1 Production and radiochemical separation of $^{103}\mbox{Ru}$

The production routes for obtaining 103Ru are highlighted in Table 6. The measured excitation function in Ditroi et al. (231) demonstrated a maximum cross-section of 10.6 ± 1.2 mb at 13.8 ± 0.6 MeV, then gradually declined and plateaued between 18 and 40 MeV, with cross sections ranging from 0.5 to 5 mb (231). The experimental results aligned closely with earlier measurements by Graf and Munzel (234) and Esterlund and Pate (244), though discrepancies in peak values were observed across the studies (231). TENDL-2011 (49) underestimated the experimental cross-sections and exhibited a shift towards the lower energies for the maximum, while EMPIRE-3.1 (96) better replicated the shape of the curve but slightly overestimated the maximum value (231). Integral yield data indicated that α induced production of 103Ru is inefficient—due to its low crosssections—compared to ⁹⁷Ru (mentioned in 8.1.1), with practical yields falling well below the MBq/μAh range (231). Tarkanyi et al.'s (232) experiment demonstrated a rise in cross section from threshold to a peak of 15.6 ± 1.7 mb at 13.79 ± 0.6 MeV, following a gradual decline and plateau between 18 and 40 MeV, with values ranging from approximately 6.2 to 1.2 mb (232). The authors reported good agreement with the corrected data of Ditroi et al. (231) and earlier measurements by Graf and Munzel (234) and Esterlund and Pate (244), except for a discrepancy by a factor of two near the absolute maximum (232). The TENDL-2011 and TENDL-2015 (49) libraries were found to underpredict the experimental cross sections and shifted the peak position toward lower energies, whereas EMPIRE-3.1 (Rivoli) (96) best reproduced both the shape and magnitude of the experimental excitation curve (232).

Mastren et al. (245) developed a two-step chromatographic purification scheme for obtaining $^{103} Ru$ from proton irradiation on a thorium target. Elution with 30 ml of 10 M HNO $_3$ (fractions 8–15) recovered $85\pm5\%$ of $^{103} Ru$ with a radiochemical purity of 82%, where they reported main impurities of $^{117m} Sn$ and $^{125,126} Sb$ with trace amounts of $^{230,233} Pa,~^{95} Nb,$ and $^{95} Zr$ in this fraction (245). To remove those

(A) Borisova et al. (242) synthesized a peptidomimetic conjugate of natural methionine and pyridine-2,6-dicarboxylate and labeled the ligand with ⁹⁷Ru for potential radiopharmaceutical utilization. (B) One of the more promising Ru(III) anticancer complexes is BOLD-100, formerly called IT-139 or KP1339, which is undergoing clinical investigation (238). Although the structure is shown as elemental Ru, Happl et al. (243) radiosynthesized c.a. [97/103Ru]BOLD-100 described in this section.

impurities, the DGA resin was incorporated, yielding a final 103 Ru recovery of $83 \pm 5\%$ with a radiochemical purity of >99.9% (245).

Blicharska et al. (246) developed a streamlined separation process to obtain 103Ru as a surrogate for fission produced 106Ru for the utilization in brachytherapy sources. The authors explored the Ru extraction efficiency in various oxidizing solutions, reporting H₅IO₆ to demonstrate the highest conversion of Ru(III/IV) to RuO₄ with 86.1% extraction (246). The method proved to be sufficiently scalable to produce hundreds GBq of 106Ru per liter of PUREX raffinate (246). More recently, Happl et al. (243) obtained [103Ru]RuCl3• xH2O by neutron activation with the Production Neutron Activation (PNA) installation at the spallation neutron source SINQ at Paul Scherrer Institute. The irradiation occurred over a three-week period at a neutron flux of 4×10^{13} n cm⁻² s⁻¹ with five ampoules containing 40-50 mg natRuCl3• xH2O that were then dissolved in concentrated hydrochloric acid, thereby resulting in activities up to 185 MBq (3.7-4.7 MBq/mg) (243). Happl et al. (238) improved their methods by obtaining 103Ru via thermal neutron irradiation (5-10×10¹⁴ n cm⁻² s⁻¹) for 6-8 d using natRu metal foils enclosed in quart ampoules, yielding 1,049 MBq at end of irradiation (EOI). From this, c.a. ¹⁰³Ru was recovered with radiochemical yields of 81%-82% (up to 648 MBq), molar activities up to 19.4 MBq µmol⁻¹ (249 MBq ml⁻¹), and a radionuclide purity of >99.9% (238).

7.2.2 Applications of ¹⁰³Ru

Tanabe (247) reported ¹⁰³Ru scintigraphy in 37 patients with various types of malignant tumors. In the cohort of four lung cancer patients, ¹⁰³Ru failed to reliably differentiate carcinoma from inflammatory lesions under the study conditions. Wenzel et al. (248) synthesized a metallocene-based analog of iodo-

hippuran—ruthenocenoyl-glycine (ruppuran) shown in Figure 9A—and labeled it with \$^{103}\$Ru to directly compare its renal clearance kinetics with \$^{125}\$I-labeled hippuran. The authors reported similar renal and plasma clearance pattern between the two compounds (248). Moreover, they did report absorbed doses to kidney and bladder with using \$^{97}\$Ru-ruppuran as well, achieving slightly lower than that of \$^{123}\$I-hippuran, with the results of clearance studies and dose estimates encouraging further kidney scintigraphy and secretory renal function measurements regarding the \$^{97}\$Ru-labeled compound (248). Weiss et al. (249) demonstrated radiolabeled [\$^{103}\$Ru]RAPTA-C (Figure 9B) to be a promising compound for translation to clinical evaluation as it rapidly cleared from the organs and the excreted by the kidneys.

Happl et al. (243) modified a three-step synthesis—published and patented for non-radioactive BOLD-100 in 2018 (250)-of [103Ru]BOLD-100 using 1.8-4.2 MBq/mg c.a. [103Ru]RuCl₃, obtaining a >93% radiochemical purity of all three compounds and >38% overall radiochemical yield in the final product. Cytotoxicity of BOLD-100 and [103Ru]BOLD-100 were compared in human colon carcinoma (HCT116) and murine colon carcinoma (CT26) cell lines using the colorimetric MTT assay with an exposure time of 96 h (243). The authors reported no effects to the biological activity in vitro even at low specific activities of 0.5-1.4 MBq/mg for [103Ru]BOLD-100 (243). Furthermore, biodistributions studies with both BOLD-100 and [103Ru]BOLD-100 were conducted in Balb/c mice bearing CT26 allografts over a period of 72 h (243). The authors reported from their tissue distribution studies that sub-equimolar amounts of c.a. [103Ru]BOLD-100 achieved a higher and prolonged tumor uptake over 72 h, establishing a potential theragnostic approach with 103Ru and 97Ru once diagnostic SPECT imaging studies with c.a. [97Ru]BOLD-100 are performed (238).

(A) (B)
$$\begin{array}{c} CO - H - H_2 \\ CO - N - C - COOH \\ \hline \\ Ru \\ H \end{array}$$

FIGURE 9

(A) Synthesizing a metallocene analog of iodo-labeled (hippuran), ruthenocenoly-glucine (ruppuran), wenzel et al. (248) injected $^{97/103}$ Ru-labeled ruppuran in rabbits. (B) Weiss et al. (249) demonstrated the prototype compound, [Ru(η^6 -p-cymene)Cl₂(pta)], where pta = 1,3,5-triaza-7-phosphaadamantane (RAPTA-C), reduces the growth of primary tumors in preclinical models for ovarian and colorectal carcinomas while being radiolabeled with 103 Ru. Both chemical structures show elemental ruthenium.

8 Discussion

In this review, we discussed eleven PGM radionuclides—¹⁹¹Pt, ^{193m}Pt, ^{195m}Pt, ¹⁰³Pd, ¹⁰⁹Pd, ^{103m}Rh, ¹⁰⁵Rh, ¹⁹¹Os, ¹⁹²Ir, ⁹⁷Ru, and 103Ru—that offer unique nuclear characteristics involving their half-lives, decay modes, and coordination chemistry suited to both diagnostic imaging and TRT. Across the radionuclides, we address two overarching themes: (1) production and separation challenges or solutions that require high specific activity and radionuclidic purity, and (2) introducing novel chelators and implementing strategies to utilize a specific radionuclide effectively. The optimal production route balances the yield, specific activity, and managing radionuclidic impurities accordingly. Reactor-based methods yield high activities but are often composed of carrier-added products, whereas accelerator routes deliver n.c.a. production—for example, 191Pt via natIr(p, xn) and 103 Ru via $^{\text{nat}}$ Mo(α ,x)—at the expense of enriched targets and complex target dissolution methods. Innovative in vivo generator systems, most notably, 103Pd/103mRh, 103Ru/103mRh, and 109Pd/109mAg show promise for implementing short-lived radionuclides; however, must overcome yield limitations relative to established generators clinically: ⁸⁸Ge/⁸⁸Ga, ⁴⁴Ti/⁴⁴Sc, ⁶²Zn/⁶²Cu, and ⁷²Se/⁷²As (118, 181, 251). Moreover, emerging nanoparticle-based brachytherapy with 103Pd and 109Pd and theragnostic applications of 195mPt-labeled complexes highlights the potential for seamless diagnostic-to-therapy transitions without altering compound pharmacokinetics. As future avenues for personalized theragnostics are of importance, platinum-based radionuclides that may offer suitable characteristics but were not mentioned in detail for this review were 188 Pt ($t_{1/2} = 10.2$ d), 189 Pt ($t_{1/2} = 10.87 \text{ h}$), and 197 Pt ($t_{1/2} = 0.83 \text{ d}$) (252). Preliminary production and chemical separation methods have been explored regarding these radionuclides, highlighted particularly in Bonardi et al. (21), Neves et al. (253), Smith et al. (252), and Wren et al. (254).

The future for PGM radionuclides may not be mainstream in the clinic; however, the recent research trends towards an optimistic future, especially regarding the radionuclides that were discussed in this review. Over the past decade, there have been notable progressions with differing radionuclides, whether through demonstration of optimal production routes and conditions, innovative separation techniques, or implementation of novel compounds for in vivo or in vitro studies. However, there are key components that deserve attention. One of the motivations is scaling up production and accessibility, as these radionuclides are produced by not only different target material but also different production pathways which makes this continued development critical. However, from this review, we have seen researchers make progress in optimizing production for certain radionuclides, yielding high specific activities that are feasible for clinical studies. Furthermore, improvements regarding radiochemical separation and recycling methods need to be of focus for cost-effective production and automative radiochemical workflows. We have seen established radiochemical separation techniques carried out to ensure high purity and yields, along with recycling of costly enriched targets to be achievable with minimal loss of enrichment (192). As future work continues to expand upon radiochemistry, the recovery of PGMs post-irradiation, minimizing radioactive waste, and developing automated separation systems may enable sustainability-economically and environmentally-for routine PGM radionuclide use later down the line. A more exciting, future component of PGM radionuclides is integrating them with novel classes of targeting agents-potentially those that have not yet been explored—that would be essential in broadening the toolkit for radiopharmaceuticals. Lastly, the pathway to mainstream adoption of PGM radionuclides will require clinical evidence of safety and efficacy.

To expand upon ¹⁹¹Pt's potential, improvements are needed in scaling up production on enriched iridium targets, along with developing automative dissolution/separation techniques to ensure reliable, high specific activity supply. Optimizing irradiation parameters will be required to elevate the small batch yields achieved for ^{193m}Pt, while *in vivo* evaluations of ^{193m}Pt-labeed complexes should be explored upon their therapeutic

efficacy, DNA damage profiles, and off-target toxicity. As Aalbersberg et al. (72) noted, enhanced purification protocols need to be developed for 195mPt, while taking advantage of its unique characteristics may open future opportunities in theragnostics. While nanoparticle-based approaches for ¹⁰³Pd are showing promise, future work must focus on taking the next step from preclinical to clinical studies, while validating dosimetry, biodistribution, and long-term safety. Like 103Pd, ¹⁰⁹Pd-porphyrin and nanoparticle-based approaches require extensive investigation in vivo stability, tumor uptake, and scaleup of n.c.a. ¹⁰⁹Pd production to support clinical studies. To exploit 103mRh's Auger emissions, efforts should focus on improving both 103Ru/103mRh and 103Pd/103mRh in vivo generators, while optimizing elution efficiencies and conducting preclinical studies to validate its therapeutic capabilities. Advancing 105Rh as a therapeutic radionuclide will require chelators capable of maximizing tumor targeting and minimizing retention, along with scale up of carrier-free routes to enable groundbreaking efficacy and toxicity studies. Streamlining osmium target dissolution and Os/Ir separation while minimizing 192Ir impurities—will be critical in advancing ¹⁹¹Os/^{191m}Ir generators, while working towards conducting preclinical studies that could translate to clinical utilization. Developing cyclotron-based routes for n.c.a. 192Ir with increased specific activity would revolutionize source availability, along with exploring novel complexes that may open new avenues beyond conventional HDR brachytherapy. Both 97Ru and 103Ru will require continued optimization of production and separation methods to support the design of matched pair theragnostics with further in vivo targeting imaging performance.

In conclusion, we provide a comprehensive review of platinum group metals that have been explored upon over the years, or those that are beginning to make their mark in nuclear medicine applications. These radionuclides offer essential nuclear characteristics that can elevate current areas of necessities, complimenting traditional radionuclides that are utilized in clinical practice. For patients, this could mean more precise imaging options, more effective treatments with fewer side effects, and personalized radiotherapy; therefore, extending the lifespan for someone. As we look ahead, the potential for PGM implementation continues to be promising. With continued efforts from across the world, what was once considered a luxurious dream in nuclear medicine may well become a future breakthrough for diagnostic imaging and cancer therapy with PGMs leading the way.

References

- Sung H, Ferlay J, Siegel RL, Laversanne M, Soerjomataram I, Jemal A, et al. Global cancer statistics 2020: GLOBOCAN estimates of incidence and mortality worldwide for 36 cancers in 185 countries. CA Cancer J Clin. (2021) 71(3):209–49. doi: 10.3322/caac.21660
- 2. Vaidya SP, Gadre S, Kamisetti RT, Patra M. Challenges and opportunities in the development of metal-based anticancer theranostic agents. *Biosci Rep.* (2022) 42(5): BSR20212160. doi: 10.1042/BSR20212160

Author contributions

DR: Writing – review & editing, Writing – original draft. IC: Writing – review & editing.

Funding

The author(s) declare that financial support was received for the research and/or publication of this article. Financial support from the Department of Nuclear Engineering at the University of Tennessee, Knoxville was received to publish this work.

Acknowledgments

We would like to thank the Department of Nuclear Engineering at the University of Tennessee, Knoxville.

Conflict of interest

The authors declare that the research was conducted in the absence of any commercial or financial relationships that could be construed as a potential conflict of interest.

Generative AI statement

The author(s) declare that no Generative AI was used in the creation of this manuscript.

Any alternative text (alt text) provided alongside figures in this article has been generated by Frontiers with the support of artificial intelligence and reasonable efforts have been made to ensure accuracy, including review by the authors wherever possible. If you identify any issues, please contact us.

Publisher's note

All claims expressed in this article are solely those of the authors and do not necessarily represent those of their affiliated organizations, or those of the publisher, the editors and the reviewers. Any product that may be evaluated in this article, or claim that may be made by its manufacturer, is not guaranteed or endorsed by the publisher.

- 3. Ntekim A, Adenipekun A, Akinlade B, Campbell O. High dose rate brachytherapy in the treatment of cervical cancer: preliminary experience with cobalt 60 radionuclide source-a prospective study. *Clin Med Insights Oncol.* (2010) 4:89–94. doi: 10.4137/CMO.S5269
- 4. Cennamo G, Montorio D, D' Andrea L, Farella A, Matano E, Giuliano M, et al. Long-term outcomes in uveal melanoma after ruthenium-106 brachytherapy. *Front Oncol.* (2022) 11:1–6. doi: 10.3389/fonc.2021.754108

- 5. Hartley FR. Chemistry of the platinum group metals: recent developments (1991).
- $6.\ Higgins\ S.\ Regarding$ ruthenium. Nat Chem. (2010) 2(12):1100. doi: 10.1038/ nchem.917
- 7. Medici S, Peana M, Nurchi VM, Lachowicz JI, Crisponi G, Zoroddu MA. Noble metals in medicine: latest advances. *Coord Chem Rev.* (2015) 284:329–50. doi: 10. 1016/j.ccr.2014.08.002
- 8. Romani AMP. Cisplatin in cancer treatment. *Biochem Pharmacol.* (2022) 206:115323. doi: 10.1016/j.bcp.2022.115323
- 9. Kapdi AR, Fairlamb IJ. Anti-cancer palladium complexes: a focus on PdX 2 L 2, palladacycles and related complexes. *Chem Soc Rev.* (2014) 43(13):4751–77. doi: 10.1039/C4CS00063C
- 10. Coskun MD, Ari F, Oral AY, Sarimahmut M, Kutlu HM, Yilmaz VT, et al. Promising anti-growth effects of palladium (II) saccharinate complex of terpyridine by inducing apoptosis on transformed fibroblasts *in vitro. Bioorg Med Chem.* (2013) 21(15):4698–705. doi: 10.1016/j.bmc.2013.05.023
- 11. Lazarević T, Rilak A, Bugarčić ŽD. Platinum, palladium, gold and ruthenium complexes as anticancer agents: current clinical uses, cytotoxicity studies and future perspectives. Eur J Med Chem. (2017) 142:8–31. doi: 10.1016/j.ejmech.2017.04.007
- 12. Husain K, Abid M, Azam A. Synthesis, characterization and antiamoebic activity of new indole-3-carboxaldehyde thiosemicarbazones and their pd (II) complexes. *Eur J Med Chem.* (2007) 42(10):1300–8. doi: 10.1016/j.ejmech. 2007.02.012
- 13. Icsel C, Yilmaz VT, Ari F, Ulukaya E, Harrison WT. Trans-dichloridopalladium (II) and platinum (II) complexes with 2-(hydroxymethyl) pyridine and 2-(2-hydroxyethyl) pyridine: synthesis, structural characterization, DNA binding and *in vitro* cytotoxicity studies. *Eur J Med Chem*. (2013) 60:386–94. doi: 10.1016/j.ejmech.2012.12.002
- Mishra A, Kaushik N. Synthesis, characterization, cytotoxicity, antibacterial and antifungal evaluation of some new platinum (IV) and palladium (II) complexes of thiodiamines. Eur J Med Chem. (2007) 42(10):1239–46. doi: 10.1016/j.ejmech.2007. 03.017
- 15. Ma D-L, Wang M, Mao Z, Yang C, Ng C-T, Leung C-H. Rhodium complexes as therapeutic agents. *Dalton Trans.* (2016) 45(7):2762–71. doi: 10.1039/C5DT04338G
- 16. Konkankit CC, Marker SC, Knopf KM, Wilson JJ. Anticancer activity of complexes of the third row transition metals, rhenium, osmium, and iridium. *Dalton Trans.* (2018) 47(30):9934–74. doi: 10.1039/C8DT01858H
- 17. Hanif M, Babak MV, Hartinger CG. Development of anticancer agents: wizardry with osmium. *Drug Discov Today*. (2014) 19(10):1640–8. doi: 10.1016/j. drudis.2014.06.016
- 18. Meier-Menches SM, Gerner C, Berger W, Hartinger CG, Keppler BK. Structure–activity relationships for ruthenium and osmium anticancer agents–towards clinical development. *Chem Soc Rev.* (2018) 47(3):909–28. doi: 10.1039/C7CS00332C
- 19. Chadwick MB, Oblozinsky P, Herman M, Greene NM, McKnight RD, Smith DL, et al. ENDF/B-VII.0: next generation evaluated nuclear data library for nuclear science and technology. *Nucl Data Sheets*. (2006) 107(12):2931–3118. doi: 10.1016/j.nds.2006.11.001
- 20. Obata H, Khandaker MU, Furuta E, Nagatsu K, Zhang M-R. Excitation functions of proton- and deuteron-induced nuclear reactions on natural iridium for the production of 191Pt. *Appl Radiat Isot.* (2018) 137:250–60. doi: 10.1016/j. apradiso.2018.03.021
- 21. Bonardi M, Birattari C, Gallorini M, Groppi F, Arginelli D, Gini L. Cyclotron production, radiochemical separation and quality control of platinum radiotracers for toxicological studies. *J Radioanal Nucl Chem.* (1998) 236(1):159–64. doi: 10.1007/BF02386335
- 22. Parent M, Strijckmans K, Cornelis R, Dewaele J, Dams R. Production of 191Pt radiotracer with high specific activity for the development of preconcentration procedures. *Nucl Instrum Methods Phys Res B*. (1994) 86(3):355–66. doi: 10.1016/0168-583X(94)95301-5
- 23. Sharma HL, Smith AG. The short-lived radioisotope production program at Manchester. *J Radioanal Chem.* (1981) 64(1):249–55. doi: 10.1007/BF02518355
- 24. Obata H, Minegishi K, Nagatsu K, Zhang M-R, Shinohara A. Production of 191Pt from an iridium target by vertical beam irradiation and simultaneous alkali fusion. *Appl Radiat Isot.* (2019) 149:31–7. doi: 10.1016/j.apradiso.2019.04.007
- 25. Areberg J, Björkman S, Einarsson L, Frankenberg B, Lundqvist H, Mattsson S, et al. Gamma camera imaging of platinum in tumours and tissues of patients after administration of 191Pt-cisplatin. *Acta Oncol.* (1999) 38(2):221–8. doi: 10.1080/028418699431654
- 26. Hoeschele JD, Butler TA, Roberts JA, Guyer CE. Analysis and refinement of the microscale synthesis of the 195mPt-labeled antitumor drug, cisdichlorodiammineplatinum (Il), cis-DDP. *Radiochim Acta*. (1982) 31(1-2):27–36. doi: 10.1524/ract.1982.31.12.27
- 27. Areberg J, Norrgren K, Mattsson S. Absorbed doses to patients from 191Pt-, 193mPt- and 195mPt-cisplatin. *Appl Radiat Isot*. (1999) 51(5):581–6. doi: 10.1016/S0969-8043(99)00082-2

- 28. Lange RC, Spencer RP, Harder HC. The antitumor agent cis-pt(NH 3) 2 cl 2: distribution studies and dose calculations for 193 m pt and 195 m pt. *J Nucl Med.* (1973) 14(4):191–5.
- 29. Obata H, Minegishi K, Nagatsu K, Ogawa M, Zhang M-R. Synthesis of no-carrier-added [188, 189, 191Pt]cisplatin from a cyclotron produced 188, 189, 191PtCl42— complex. *Sci Rep.* (2021) 11(1):8140. doi: 10.1038/s41598-021-87576-2
- 30. Obata H, Tsuji AB, Sudo H, Sugyo A, Minegishi K, Nagatsu K, et al. *In vitro* evaluation of no-carrier-added radiolabeled cisplatin ([(189, 191)Pt]cisplatin) emitting auger electrons. *Int J Mol Sci.* (2021) 22(9):4622–36. doi: 10.3390/iime22064622
- 31. Obata H, Tsuji AB, Kumata K, Sudo H, Minegishi K, Nagatsu K, et al. Development of novel 191Pt-labeled Hoechst33258: 191Pt is more suitable than 111In for targeting DNA. *J Med Chem.* (2022) 65(7):5690–700. doi: 10.1021/acs. imedchem.1c02209
- 32. Vallis KA, Reilly RM, Scollard D, Merante P, Brade A, Velauthapillai S, et al. Phase I trial to evaluate the tumor and normal tissue uptake, radiation dosimetry and safety of (111)In-DTPA-human epidermal growth factor in patients with metastatic EGFR-positive breast cancer. *Am J Nucl Med Mol Imaging.* (2014) 4(2):181–92.
- 33. De Jong M, Valkema R, Jamar F, Kvols LK, Kwekkeboom DJ, Breeman WA, et al. Somatostatin receptor-targeted radionuclide therapy of tumors: preclinical and clinical findings. *Semin Nucl Med.* (2002) 32(2):133–40. doi: 10.1053/snuc. 2002.31027
- 34. Cai Z, Chattopadhyay N, Yang K, Kwon YL, Yook S, Pignol JP, et al. (111)Inlabeled trastuzumab-modified gold nanoparticles are cytotoxic *in vitro* to HER2-positive breast cancer cells and arrest tumor growth *in vivo* in athymic mice after intratumoral injection. *Nucl Med Biol.* (2016) 43(12):818–26. doi: 10.1016/j. nucmedbio.2016.08.009
- 35. Obata H, Tsuji AB, Sudo H, Sugyo A, Hashiya K, Ikeda H, et al. Novel auger-electron-emitting 191Pt-labeled pyrrole-imidazole polyamide targeting MYCN increases cytotoxicity and cytosolic dsDNA granules in MYCN-amplified neuroblastoma. *Pharmaceuticals*. (2023) 16(11):1526. doi: 10.3390/ph16111526
- 36. Hidaka T, Tsubono Y, Hashiya K, Bando T, Pandian GN, Sugiyama H. Enhanced nuclear accumulation of pyrrole-imidazole polyamides by incorporation of the tri-arginine vector. *Chem Commun.* (2020) 56(82):12371–4. doi: 10.1039/D0CC05158F
- 37. Yu Z, Pandian GN, Hidaka T, Sugiyama H. Therapeutic gene regulation using pyrrole-imidazole polyamides. *Adv Drug Delivery Rev.* (2019) 147:66–85. doi: 10. 1016/j.addr.2019.02.001
- 38. Igarashi J, Fukuda N, Inoue T, Nakai S, Saito K, Fujiwara K, et al. Preclinical study of novel gene silencer pyrrole-imidazole polyamide targeting human TGF-β1 promoter for hypertrophic scars in a common marmoset primate model. *PLoS One.* (2015) 10(5):e0125295. doi: 10.1371/journal.pone.0125295
- 39. Yoda H, Inoue T, Shinozaki Y, Lin J, Watanabe T, Koshikawa N, et al. Direct targeting of MYCN gene amplification by site-specific DNA alkylation in neuroblastoma. *Cancer Res.* (2019) 79(4):830–40. doi: 10.1158/0008-5472.CAN-18-1198
- 40. Omokawa M, Kimura H, Hatsukawa Y, Kawashima H, Tsukada K, Yagi Y, et al. Production and synthesis of a novel 191Pt-labeled platinum complex and evaluation of its biodistribution in healthy mice. *Bioorg Med Chem.* (2024) 97:117557. doi: 10. 1016/j.bmc.2023.117557
- 41. Omokawa M, Kimura H, Arimitsu K, Yagi Y, Hattori Y, Kawashima H, et al. Synthesis and biological evaluation of a novel sugar-conjugated platinum(II) Complex having a tumor-targeting effect. ACS Omega. (2024) 9(1):879–86. doi: 10.1021/acsomega.3c06922
- 42. Obata H, Tsuji AB, Feng Y, Zheng Y, Sudo H, Sugyo A, et al. Trithiol ligand provides tumor-targeting 191Pt-complexes with high molar activity and promising *in vivo* properties. *Nucl Med Biol.* (2025) 146-147:109043. doi: 10.1016/j. nucmedbio.2025.109043
- 43. Wawrowicz K, Majkowska-Pilip A, Gaweł D, Chajduk E, Pieńkowski T, Bilewicz A. Au@pt core-shell nanoparticle bioconjugates for the therapy of HER2+ breast cancer and hepatocellular carcinoma. Model studies on the applicability of (193 m)Pt and (195 m)Pt radionuclides in auger electron therapy. *Molecules*. (2021) 26(7):2051–70. doi: 10.3390/molecules26072051
- 44. Uddin MS, Scholten B, Hermanne A, Sudár S, Coenen HH, Qaim SM. Radiochemical determination of cross sections of α -particle induced reactions on 192Os for the production of the therapeutic radionuclide 193mPt. *Appl Radiat Isot.* (2010) 68(10):2001–6. doi: 10.1016/j.apradiso.2010.05.002
- 45. Hilgers K, Coenen HH, Qaim SM. Production of the therapeutic radionuclides 193mPt and 195mPt with high specific activity via alpha-particle-induced reactions on 192Os. *Appl Radiat Isot.* (2008) 66(4):545–51. doi: 10.1016/j.apradiso.2007.10.009
- 46. Stuchbery AE. Electrodeposition of pt and os targets for nuclear reaction experiments. *Nucl Instrum Methods Phys Res.* (1983) 211(2-3):293–5. doi: 10.1016/0167-5087(83)90250-8
- 47. Chakrabarty S, Tomar BS, Goswami A, Raman VA, Manohar SB. Preparation of thin osmium targets by electrodeposition. *Nucl Instrum Methods Phys Res B.* (2001) 174(1):212–4. doi: 10.1016/S0168-583X(00)00509-7

- 48. Jones T. Electrodeposition of osmium. Metal Finish. (2002) 100(6):84–90. doi: 10.1016/S0026-0576(02)80443-3
- 49. Koning AJ, Rochman D. Modern nuclear data evaluation with the TALYS code system. *Nucl Data Sheets*. (2012) 113(12):2841–934. doi: 10.1016/j.nds.2012.11.002
- 50. Uhl M, Strohmaier B. STAPRE: A computer code for particle induced activation cross sections and related quantities: Institut für Radiumforschung und Kernphysik der Österreichischen Akademie (1976)
- 51. Uddin MS, Hermanne A, Scholten B, Spellerberg S, Coenen HH, Qaim SM. Small scale production of high purity ^{193}mPt by the $^{192}\text{Os}(\alpha,3\text{n})\text{-process}.$ Radiochim Acta. (2011) 99(3):131–5. doi: 10.1524/ract.2011.1807
- 52. Azure MT, Sastry KS, Archer RD, Howell R, Rao DV. Microscale synthesis of carboplatin labeled with the Auger emitter platinum-193m: Radiotoxicity versus chemotoxicity of the antitumor drug in mammalian cells. Biophysical aspects of Auger processes American Association of Physicists in Medicine symposium proceedings No 8 (1992).
- 53. Ahmed N, Koch KR. The liquid—liquid extraction of platinum in the presence of tin (II) chloride from dilute hydrochloric acid into 4-methyl-2-pentanone. *Anal Chim Acta*. (1984) 162:347–56. doi: 10.1016/S0003-2670(00)84256-7
- 54. Koch KR, Yates JE. The effect of tin (II) chloride on the liquid-liquid extraction of tetrachloroplatinate (II) ions by triphenylphosphine in dichloromethane. *Anal Chim Acta*. (1983) 147:235–45. doi: 10.1016/0003-2670(83)80089-0
- 55. Lange RC, Spencer RP, Harder HC. Synthesis and distribution of a radiolabeled antitumor agent: cis-diamminedichloroplatinum (II). *J Nucl Med.* (1972) 13(5):328–30.
- 56. Howell RW. Radiobiological Effects of Auger Electrons in the Decay of Pt-195 m. Amherst, MA, United States: University of Massachusetts (1987).
- 57. Wawrowicz K, Bilewicz A. Challenging production of auger electron emitter platinum-195 m via double-neutron capture activation of an iridium-193 target. *Bio-Algorithms Med-Systems*. (2023) 19:35–9. doi: 10.5604/01.3001.0054.1821
- 58. Ferrari G, Lopez-Martinez I, Wanek T, Kuntner C, Montagner D. Recent advances on pt-based compounds for theranostic applications. *Molecules*. (2024) 29(15):3453–85. doi: 10.3390/molecules29153453
- 59. Knapp FF Jr, Mirzadeh S, Beets AL, Du M. Production of therapeutic radioisotopes in the ORNL HighFlux isotope reactor (HFIR) for applications in nuclear medicine, oncologyandinterventional cardiology. *J Radioanal Nucl Chem.* (2005) 263(2):503–9. doi: 10.1007/s10967-005-0083-4
- 60. Mirzadeh S, Knapp F Jr, Alexander C, Mausner L. Evaluation of neutron inelastic scattering for radioisotope production. *Appl Radiat Isot.* (1997) 48(4):441–6. doi: 10.1016/S0969-8043(96)00284-9
- 61. Siegfried C, Weinert W, Strelow F, Böhmer RG. Cation-exchange in thiourea-hydrochloric acid solutions. *Talanta*. (1983) 30(6):413–8. doi: 10.1016/0039-9140(83) 80097-6
- 62. Berg EW, Senn WL Jr. Ion exchange separation of rhodium and iridium. *Anal Chem.* (1955) 27(8):1255–6. doi: 10.1021/ac60104a013
- Akaboshi M. Platinum 195m: in manual for reactor produced radioisotopes. IAEA-TECDOC-1340 (2003).
- 64. Vosoughi S, Rovias MRA, Rahiminezhad A, Novin FB, Yousefi K, Sardjono Y. Production assessment of 195mPt in Tehran research reactor. *J Radioanal Nucl Chem.* (2023) 332(8):2989–94. doi: 10.1007/s10967-023-09008-x
- 65. Vimalnath KV, Chakraborty S, Dash A. Reactor production of no-carrier-added 199Au for biomedical applications. *RSC Adv.* (2016) 6(86):82832–41. doi: 10.1039/C6RA15407G
- 66. Zeevaart JR, Wagener J, Marjanovic-Painter B, Sathekge M, Soni N, Zinn C, et al. Production of high specific activity (195 m) pt-cisplatinum at South African nuclear energy corporation for phase 0 clinical trials in healthy individual subjects. *J Labelled Comp Radiopharm*. (2013) 56(9-10):495–503. doi: 10.1002/jlcr.3091
- 67. Bodnar EN, Dikiy MP, Medvedeva EP. Photonuclear production and antitumor effect of radioactive cisplatin (195mPt). *J Radioanal Nucl Chem.* (2015) 305(1):133–8. doi: 10.1007/s10967-015-4053-1
- $\,$ 68. Smith SV. Methods of synthesis and use of radiolabelled platinum chemotherapeutic agents. Google Patents (2006).
- 69. Sathekge M, Wagener J, Smith SV, Soni N, Marjanovic-Painter B, Zinn C, et al. Biodistribution and dosimetry of 195mPt-cisplatin in normal volunteers. *Imaging Agent Single Photon Emission Comput Tomography*. (2013) 52(06):222–7. doi: 10. 3413/Nukmed-0599-13-06
- 70. Chernyaev I. Synthesis of complex compounds of Platinum group metals. Reference book (1964).
- 71. Dykiy MP, Dovbnya AN, Lyashko YV, Medvedeva EP, Medvedev DV, Uvarov VL. Photonuclear production of 193 m, 195mPt and synthesis of radioactive cisplatin. J Label Compd Radiopharm. (2007) 50(5-6):480–2. doi: 10.1002/jlcr.1210
- 72. Aalbersberg EA, de Wit van der Veen BJ, Zwaagstra O, Codée van der Schilden K, Vegt E, Vogel WV. Preclinical imaging characteristics and quantification of platinum-195 m SPECT. *Eur J Nucl Med Mol Imaging.* (2017) 44(8):1347–54. doi: 10.1007/s00259-017-3643-2

- 73. Muns JA, Montserrat V, Houthoff H-J, Codée-van der Schilden K, Zwaagstra O, Sijbrandi NJ, et al. *In vivo* characterization of platinum(II)-based linker technology for the development of antibody-drug conjugates: taking advantage of dual labeling with ^{195m}Pt and ⁸⁹Zr. *J Nucl Med.* (2018) 59(7):1146–51. doi: 10.2967/jnumed.117.206672
- 74. Nadar RA, Farbod K, der Schilden KC, Schlatt L, Crone B, Asokan N, et al. Targeting of radioactive platinum-bisphosphonate anticancer drugs to bone of high metabolic activity. *Sci Rep.* (2020) 10(1):5889. doi: 10.1038/s41598-020-62039-2
- 75. Margiotta N, Ostuni R, Teoli D, Morpurgo M, Realdon N, Palazzo B, et al. Bisphosphonate complexation and calcium doping in silica xerogels as a combined strategy for local and controlled release of active platinum antitumor compounds. *Dalton Trans.* (2007) 29:3131–9. doi: 10.1039/b705239a
- 76. Nadar RA, Franssen GM, Van Dijk NWM, Codee-van der Schilden K, de Weijert M, Oosterwijk E, et al. Bone tumor-targeted delivery of theranostic 195mPt-bisphosphonate complexes promotes killing of metastatic tumor cells. *Materials Today Bio.* (2021) 9:100088. doi: 10.1016/j.mtbio.2020.100088
- 77. de Roest RH, Stigter van Walsum M, van der Schilden K, Brakenhoff RH. Pharmacodynamics and biodistribution of [195mPt]cisplatin(CISSPECT[®]) in head and neck squamous cell carcinoma. *EJNMMI Res.* (2024) 14(1):22. doi: 10.1186/s13550-024-01082-w
- 78. Boros E, Packard AB. Radioactive transition metals for imaging and therapy. Chem Rev. (2019) 119(2):870–901. doi: 10.1021/acs.chemrev.8b00281
- 79. Hussain M, Sudar S, Aslam MN, Shah HA, Ahmad R, Malik AA, et al. A comprehensive evaluation of charged-particle data for production of the therapeutic radionuclide 103Pd. *Appl Radiat Isot.* (2009) 67(10):1842–54. doi: 10. 1016/j.apradiso.2009.06.010
- 80. Sudár S, Cserpák F, Qaim SM. Measurements and nuclear model calculations on proton-induced reactions on 103Rh up to 40MeV: evaluation of the excitation function of the 103Rh(p,n)103Pd reaction relevant to the production of the therapeutic radionuclide 103Pd. *Appl Radiat Isot.* (2002) 56(6):821–31. doi: 10.1016/S0969-8043(02)00054-4
- 81. Albert RD. (\$p, n\$) cross section and proton optical-model parameters in the 4-to 5.5-mev energy region. *Phys Rev.* (1959) 115(4):925–7. doi: 10.1103/PhysRev.115.
- 82. Johnson C, Galonsky A, Inskeep C. Cross sections for (p, n) reactions in intermediate-weight nuclei. *Phys Rev A*. (1960) 136:B1719–B29. doi: 10.1103/PhysRev.136.B1719
- 83. Hansen LF, Albert RD. Statistical theory predictions for 5-to 11-MeV (p,n) and (p,p') nuclear reactions in V 51, co 59, cu 63, cu 65, and rh 103. *Phys Rev.* (1962) 128(1):291. doi: 10.1103/PhysRev.128.291
- 84. Blaser J, Boehm F, Marmier P, Scherrer P. Anregungsfunktionen und wirkungsquerschnitte der (P, N)-reaktion. 2. *Helvetica Phys Acta*. (1951) 24(5):441–64.
- 85. Harper P, Lathrop K, Need J. The thick target yield and excitation function for the reaction Rh \$ sup 103\$(pn) Pd \$ sup 10\$\$ sup 3\$. Chicago. Univ.; and Argonne Cancer Research Hospital, Chicago; Oak Ridge (1961).
- $86.\ Treytl$ W, Caretto A Jr. Study of (p, n) reactions between 100 and 400 MeV. Phys Rev. 1966;146(3):836. doi: 10.1103/PhysRev.146.836
- 87. Mukhammedov S, Vasidov A. Determination of rhodium by proton-activation technique using the (p, n) reaction at a cyclotron. *Izv Akad Nauk Uzb SSR*, *Ser Fiz Mat.* (1984) 2:329.
- 88. Hermanne A, Sonck M, Fenyvesi A, Daraban L. Study on production of 103Pd and characterisation of possible contaminants in the proton irradiation of 103Rh up to 28 MeV. *Nucl Instrum Methods Phys Res B.* (2000) 170(3-4):281–92. doi: 10.1016/S0168-583X(00)00190-7
- 89. Fassbender M, Nortier F, Schroeder I W, Van Der Walt T. The production of 103Pd via the natAg (p, x) 103Pd nuclear process. *Radiochim Acta*. (1999) 87(3-4):87–92. doi: 10.1524/ract.1999.87.34.87
- 90. Uddin M, Hagiwara M, Baba M, Tarkanyi F, Ditroi F. Experimental studies on excitation functions of the proton-induced activation reactions on yttrium. *Appl Radiat Isot.* (2005) 63(3):367–74. doi: 10.1016/j.apradiso.2005.04.006
- 91. Uddin MS, Baba M, Hagiwara M, Latif S, Qaim SM. Excitation functions for the formation of some short-lived products in proton-induced reactions on silver. *Radiochim Acta*. (2008) 96(2):67–72. doi: 10.1524/ract.2008.1468
- 92. Hermanne A, Sonck M, Takács S, Tárkányi F, Shubin Y. Study on alternative production of 103Pd and characterisation of contaminants in the deuteron irradiation of 103Rh up to 21 MeV. *Nucl Instrum Methods Phys Res B.* (2002) 187(1):3–14. doi: 10.1016/S0168-583X(01)00851-5
- 93. Hermanne A, Sonck M, Takács S, Tárkányi F, Shubin Y. Deuteron bombardment of 103Rh: a new promising pathway for the production of 103Pd. *J Nucl Sci Technol.* (2002) 39(sup2):1286–9. doi: 10.1080/00223131.2002.10875339
- 94. Skakun Y, Qaim SM. Excitation Functions of Helion-Induced Nuclear Reactions for the Production of the Medical Radioisotope 103Pd. AIP Conference Proceedings; American Institute of Physics (2005).
- 95. Skakun Y, Qaim S. Measurement of excitation functions of helion-induced reactions on enriched ru targets for production of medically important 103Pd and

- 101mRh and some other radionuclides. Appl Radiat Isot. (2008) 66(5):653–67. doi: 10.1016/j.apradiso.2007.11.013
- 96. Herman M, Capote R, Carlson BV, Obložinský P, Sin M, Trkov A, et al. EMPIRE: nuclear reaction model code system for data evaluation. *Nucl Data Sheets.* (2007) 108(12):2655–715. doi: 10.1016/j.nds.2007.11.003
- 97. Tárkányi F, Hermanne A, Király B, Takacs S, Ditroi F, Csikai J, et al. New cross-sections for production of 103Pd; review of charged particle production routes. *Appl Radiat Isot.* (2009) 67(9):1574–81. doi: 10.1016/j.apradiso.2009.03.100
- 98. Hermanne A, Takacs S, Tárkányi F, Bolbos R. Cross section measurements of proton and deuteron induced formation of 103Ag in natural palladium. *Radiochim Acta*. (2004) 92(4-6):215–8. doi: 10.1524/ract.92.4.215.35609
- 99. Manenti S, Alí Santoro MC, Cotogno G, Duchemin C, Haddad F, Holzwarth U, et al. Excitation function and yield for the 103Rh(d,2n)103Pd nuclear reaction: optimization of the production of palladium-103. *Nucl Med Biol.* (2017) 49:30–7. doi: 10.1016/j.nucmedbio.2017.02.005
- 100. Ditrói F, Tárkányi F, Takács S, Hermanne A, Yamazaki H, Baba M, et al. Study of activation cross-sections of deuteron induced reactions on rhodium up to 40 MeV. Nucl Instrum Methods Phys Res B. (2011) 269(18):1963–72. doi: 10.1016/j.nimb.2011.
- 101. Ohya T, Nagatsu K, Minegishi K, Zhang M-R. Separation of 103Pd from a Rh target using an alloying pretreatment with bismuth. *Radiochim Acta.* (2022) 110(4):251–8. doi: 10.1515/ract-2021-1117
- 102. Krol V, Koers LM, McNeil S, Hoehr C, Radchenko V. Cyclotron production of 103Pd using a liquid target. *Nucl Med Biol.* (2023) 118-119:108328. doi: 10.1016/j.nucmedbio.2023.108328
- 103. Laouameria AN, Hunyadi M, Csík A, Szűcs Z. Innovative approach to producing palladium-103 for auger-emitting radionuclide therapy: a proof-of-concept study. *Pharmaceuticals.* (2024) 17(2):253. doi: 10.3390/ph17020253
- 104. Blasko JC, Grimm PD, Sylvester JE, Badiozamani KR, Hoak D, Cavanagh W. Palladium-103 brachytherapy for prostate carcinoma. *Int J Radiat Oncol Biol Phys.* (2000) 46(4):839–50. doi: 10.1016/S0360-3016(99)00499-X
- 105. Li Z-Y, Gao H-B, Deng X-S, Zhou L, Zhang W-H, Han L-G, et al. Preparation of 103Pd brachytherapy seeds by electroless plating of 103Pd onto carbon bars. *Appl Radiat Isot.* (2015) 103:128–30. doi: 10.1016/j.apradiso.2015.05.020
- 106. Li Z, Cui H, Gao H, Han L, Zhang W, Jin X. Study on electroless 103 pd-plating process. *Atomic Energy Sci Technol.* (2013) 47(9):1508–13. doi: 10.7538/yzk. 2013.47.09.1508
- 107. Laprise-Pelletier M, Lagueux J, Côté MF, LaGrange T, Fortin MA. Low-dose prostate cancer brachytherapy with radioactive palladium-gold nanoparticles. *Adv Healthc Mater.* (2017) 6(4):1601120–33. doi: 10.1002/adhm.201601120
- 108. Djoumessi D, Laprise-Pelletier M, Chevallier P, Lagueux J, Côté MF, Fortin MA. Rapid, one-pot procedure to synthesise 103Pd:pd@au nanoparticles en route for radiosensitisation and radiotherapeutic applications. *J Mater Chem B.* (2015) 3(10):2192–205. doi: 10.1039/C4TB01663G
- 109. Moeendarbari S, Tekade R, Mulgaonkar A, Christensen P, Ramezani S, Hassan G, et al. Theranostic nanoseeds for efficacious internal radiation therapy of unresectable solid tumors. *Sci Rep.* (2016) 6(1):20614. doi: 10.1038/srep20614
- 110. Fach M, Fliedner FP, Kempen PJ, Melander F, Hansen AE, Bruun LM, et al. Effective intratumoral retention of [103Pd] AuPd alloy nanoparticles embedded in gel-forming liquids paves the way for new nanobrachytherapy. *Adv Healthcare Mater.* (2021) 10(10):2002009. doi: 10.1002/adhm.202002009
- 111. Sporer E, Deville C, Straathof NJW, Bruun LM, Köster U, Jensen M, et al. Optimized chelator and nanoparticle strategies for high-activity 103Pd-loaded biodegradable brachytherapy seeds. *EJNMMI Radiopharm Chem.* (2024) 9(1):92. doi: 10.1186/s41181-024-00309-4
- 112. Hindié E, Larouze A, Alcocer-Ávila M, Morgat C, Champion C. Palladium-103 ((103)Pd/(103 m)Rh), a promising auger-electron emitter for targeted radionuclide therapy of disseminated tumor cells absorbed doses in single cells and clusters, with comparison to (177)Lu and (161)Tb. *Theranostics*. (2024) 14(11):4318–30. doi: 10.7150/thno.95436
- 113. Champion C, Zanotti-Fregonara P, Hindié E. CELLDOSE: a monte carlo code to assess electron dose distribution—s values for 131I in spheres of various sizes. *J Nucl Med.* (2008) 49(1):151–7. doi: 10.2967/jnumed.107.045179
- 114. Sato T, Iwamoto Y, Hashimoto S, Ogawa T, Furuta T, Abe S-I, et al. Recent improvements of the particle and heavy ion transport code system–PHITS version 3.33. *J Nucl Sci Technol.* (2024) 61(1):127–35. doi: 10.1080/00223131.2023.2275736
- 115. Annamalaisamy GP, Lyczko M, Bilewicz A. The radioactive 103 pd and 109 pd palladium bipyridyl–bisphosphonate complexes for radionuclide therapy of bone metastatic tumor cells. *RSC Adv.* (2025) 15(23):18501–11. doi: 10.1039/D5RA02172C
- 116. Cipriani M, Rostán S, León I, Li Z-H, Gancheff JS, Kemmerling U, et al. Multitarget heteroleptic palladium bisphosphonate complexes. *J Biol Inorgan Chem.* (2020) 25:509–19. doi: 10.1007/s00775-020-01779-y
- 117. Fathy AA, Butler IS, Abd Elrahman M, Jean-Claude BJ, Mostafa SI. Anticancer evaluation and drug delivery of new palladium (II) complexes based on the chelate of alendronate onto hydroxyapatite nanoparticles. *Inorg Chim Acta.* (2018) 473:44–50. doi: 10.1016/j.ica.2017.12.015

- 118. Jensen AI, Zhuravlev F, Severin G, Magnus CB, Fonslet J, Köster U, et al. A solid support generator of the auger electron emitter rhodium-103 m from [(103)Pd]palladium. *Appl Radiat Isot.* (2020) 156:108985. doi: 10.1016/j.apradiso. 2019.108985
- 119. Nath A, Prushan M, Gilbert J. Can super-excited molecules survive fragmentation? *J Radioanal Nucl Chem.* (2001) 247(3):589–91. doi: 10.1023/A:1010655215719
- 120. van Rooyen J, Szucs Z, Zeevaart JR. A possible *in vivo* generator 103Pd/103mRh—recoil considerations. *Appl Radiat Isot.* (2008) 66(10):1346–9. doi: 10.1016/j.apradiso.2008.02.088
- 121. Szucs Z, van Rooyen J, Zeevaart JR. Recoil effect on β -decaying *in vivo* generators, interpreted for 103Pd/103mRh. *Appl Radiat Isot.* (2009) 67(7-8):1401–4. doi: 10.1016/j.apradiso.2009.02.022
- 122. Zhao L, Liu S, Liang D, Jiang T, Yan X, Zhao S, et al. Resensitization of cisplatin resistance ovarian cancer cells to cisplatin through pretreatment with low-dose fraction radiation. *Cancer Med.* (2019) 8(5):2442–8. doi: 10.1002/cam4.2116
- 123. Chakraborty S, Das T, Sarma HD, Banerjee S. Effect of lipophilicity on biological properties of 109Pd-porphyrin complexes: a preliminary investigation. *J Porphyrins Phthalocyanines*. (2012) 16(01):64–71. doi: 10.1142/S1088424611004427
- 124. Fawwaz RA, Hemphill W, Winchell HS. Potential use of ¹⁰⁹Pd-porphyrin complexes for selective lymphatic ablation. *J Nucl Med.* (1971) 12(5):231–6.
- 125. Pineau J, Lima LMP, Platas-Iglesias C, Zeevaart JR, Driver CHS, Le Bris N, et al. Relevance of palladium to radiopharmaceutical development considering enhanced coordination properties of TE1PA. *Chemistry*. (2022) 28(41):e202200942. doi: 10.1002/chem.202200942
- 126. Hien NT, Kim G, Kim K, Do NV, Khue PD, Thanh KT, et al. Measurements of the thermal neutron cross-section and resonance integral for the $108Pd(n,\gamma)109Pd$ reaction. *Nucl Instrum Methods Phys Res B.* (2018) 424:37–42. doi: 10.1016/j.nimb. 2018.03.031
- 127. Farina Arbocco F, Vermaercke P, Smits K, Sneyers L, Strijckmans K. Experimental determination of k 0, Q 0 factors, effective resonance energies and neutron cross-sections for 37 isotopes of interest in NAA. *J Radioanal Nucl Chem.* (2014) 302:655–72. doi: 10.1007/s10967-014-3281-0
- 128. Krtička M, Firestone R, McNabb D, Sleaford B, Agvaanluvsan U, Belgya T, et al. Thermal neutron capture cross sections of the palladium isotopes. *Phys Rev C Nucl Phys.* (2008) 77(5):054615. doi: 10.1103/PhysRevC.77.054615
- 129. Firestone R, Krtiaka M, McNabb D, Sleaford B, Agvaanluvsan U, Belgya T, et al. Thermal neutron capture cross sections of the palladium isotopes. AIP Conference Proceedings; American Institute of Physics (2006).
- 130. Duncan C, Krane K. Neutron capture cross section of pd 102. *Phys Rev C Nucl Phys.* (2005) 71(5):054322. doi: 10.1103/PhysRevC.71.054322
- 131. De Corte F, Simonits A. K 0-measurements and related nuclear data compilation for (n, γ) reactor neutron activation analysis: iIIb: tabulation. *J Radioanal Nucl Chem.* (1989) 133:43–130. doi: 10.1007/BF02039970
- 132. Lyon W. Reactor neutron activation cross sections for a number of elements. Nucl Sci Eng. (1960) 8(5):378–80. doi: 10.13182/NSE60-A25817
- 133. Sehgal M, Hans H, Gill P. Thermal neutron cross-sections for producing some isomers. *Nucl Phys.* (1959) 12(3):261–8. doi: 10.1016/0029-5582(59)90172-5
- 134. Seren L, Friedlander HN, Turkel SH. Thermal neutron activation cross sections. *Phys Rev.* (1947) 72(10):888. doi: 10.1103/PhysRev.72.888
- 135. Van der Linden R, De Corte F, Van Den Winkel P, Hoste J. A compilation of infinite dilution resonance integrals, I. *J Radioanal Chem.* (1972) 11:133–41. doi: 10. 1007/BF02518625
- 136. Dougherty TJ, Gomer CJ, Henderson BW, Jori G, Kessel D, Korbelik M, et al. Photodynamic therapy. *J Natl Cancer Inst.* (1998) 90(12):889–905. doi: 10.1093/jnci/90.12.889
- 137. Harrod-Kim P. Tumor ablation with photodynamic therapy: introduction to mechanism and clinical applications. J Vasc Interv Radiol. (2006) 17(9):1441–8. doi: 10.1097/01.RVI.0000231977.49263.DE
- 138. Whitacre CM, Feyes DK, Satoh T, Grossmann J, Mulvihill JW, Mukhtar H, et al. Photodynamic therapy with the phthalocyanine photosensitizer pc 4 of SW480 human colon cancer xenografts in athymic mice. *Clin Cancer Res.* (2000) 6(5):2021–7.
- 139. Brown SB, Brown EA, Walker I. The present and future role of photodynamic therapy in cancer treatment. *Lancet Oncol.* (2004) 5(8):497–508. doi: 10.1016/S1470-2045(04)01529-3
- 140. Doi JD, Lavallee DK, Srivastava SC, Prach T, Richards P, Fawwaz RA. Preparation of 109Pd-hematoporphyrin for selective lymphatic ablation using N-methylhematoporphyrin. *Int J Appl Radiat Isot.* (1981) 32(12):877–80. doi: 10.1016/0020-708X(81)90071-5
- 141. Fawwaz RA, Wang TS, Srivastava SC, Rosen JM, Ferrone S, Hardy MA, et al. Potential of palladium-109-labeled antimelanoma monoclonal antibody for tumor therapy. *J Nucl Med.* (1984) 25(7):796–9.
- 142. Das T, Chakraborty S, Sarma HD, Banerjee S. A novel [109Pd] palladium labeled porphyrin for possible use in targeted radiotherapy. *Radiochim Acta*. (2008) 96(7):427–33. doi: 10.1524/ract.2008.1505

- 143. Gharibkandi NA, Wawrowicz K, Majkowska-Pilip A, Żelechowska-Matysiak K, Wierzbicki M, Bilewicz A. Au@109Pd core-shell nanoparticle conjugated to trastuzumab for the therapy of HER2+ cancers: studies on the applicability of 109Pd/109mAg *in vivo* generator in combined β auger electron therapy. *EJNMMI Radiopharm Chem.* (2023) 8(1):26. doi: 10.1186/s41181-023-00212-4
- 144. Gawęda W, Pruszyński M, Cędrowska E, Rodak M, Majkowska-Pilip A, Gaweł D, et al. Trastuzumab modified barium ferrite magnetic nanoparticles labeled with radium-223: a new potential radiobioconjugate for alpha radioimmunotherapy. *Nanomaterials (Basel)*. (2020) 10(10):2067–87. doi: 10.3390/nano10102067
- 145. Gharibkandi NA, Wawrowicz K, Walczak R, Majkowska-Pilip A, Wierzbicki M, Bilewicz A. 109Pd/109mAg *In vivo* generator in the form of nanoparticles for combined β auger electron therapy of hepatocellular carcinoma. *EJNMMI Radiopharm Chem.* (2024) 9(1):59. doi: 10.1186/s41181-024-00293-9
- 146. Agency IAE. Manual for Reactor Produced Radioisotopes: International Atomic Energy Agency (2003).
- 147. Cheng C, Treves S, Samuel A, Davis MA. A new osmium-191 \rightarrow iridium-191 m generator. *J Nucl Med.* (1980) 21(12):1169–76.
- 148. Jamre M, Salek N, Jalilian A, Moghaddam L, Shamsaei Zafarghandi M, Mazidi M, et al. Development of an *in vivo* radionuclide generator by labeling bleomycin with 191 os. *J Radioanal Nucl Chem.* (2011) 290:543–9. doi: 10.1007/s10967-011-1288-3
- 149. Salek N, Jamre M, B LM, Jalilian AR, Shamsaee M. Feasibility and improvement in production of 1910s/191mIr generator by Tehran research reactor (TRR). *Ann Nucl Energy.* (2012) 40(1):194–9. doi: 10.1016/j.anucene.2011.09.019
- 150. Brihaye C, Dewez S, Guillaume M, Callahan AP, Rice DE, Knapp FF. Reactor production and purification of osmium-191 for use in a new 1910s/191mIr radionuclide generator system. *Int J Radiat Appl Instrum A*. (1989) 40(2):183–91. doi: 10.1016/0883-2889(89)90196-2
- 151. Moghaddam-Banaem L, Jalilian A-R, Salek N, Jamreh M. Preparation of 191Os-phytate, an *in vivo* radionuclide generator, for radiosynovectomy application. *J Nucl Res Appl.* (2021) 1(1):9–17. doi: 10.24200/nep.2021.1001
- 152. Moghaddam L, Jalilian A, Jamre M, Salek N, Mazidi M, Ghannadi-Maragheh M. Radiosynthesis of 191Os-2-acetylpyridine thiosemicarbazone complex, as an *in vivo* therapeutic radionuclide generator. *Iran J Nucl Med.* (2013) 21:53–9.
- 153. Hilgers K, Sudár S, Qaim SM. Experimental study and nuclear model calculations on the 192Os(p,n)192Ir reaction: comparison of reactor and cyclotron production of the therapeutic radionuclide 192Ir. *Appl Radiat Isot.* (2005) 63(1):93–8. doi: 10.1016/j.apradiso.2004.12.010
- 154. Bertermann H, Brix F. Ultrasonically Guided Interstitial High Dose Rate Brachytherapy with Ir-192: Technique and Preliminary Results in Locally Confined Prostate Cancer. Brachytherapy HDR and LDR: Remote Afterloading State of Art Leerson. The Netherlands: Nucletron International BV (1990). p. 281–303.
- 155. Langille G, Yang H, Zeisler SK, Hoehr C, Storr T, Andreoiu C, et al. Low energy cyclotron production and cyclometalation chemistry of iridium-192. *Appl Radiat Isot.* (2016) 115:81–6. doi: 10.1016/j.apradiso.2016.06.005
- 156. Mate TP, Gottesman JE, Hatton J, Gribble M, Van Hollebeke L. High dose-rate afterloading 192Iridium prostate brachytherapy: feasibility report. *Int J Radiat Oncol Biol Phys.* (1998) 41(3):525–33. doi: 10.1016/S0360-3016(98)00097-2
- 157. Ananthakrishnan M. Iridium 192. Manual for Reactor Produced Radioisotopes IAEA-TECDOC-1340. (2003) p. 116.
- 158. Schaeken B, Vanneste F, Bouiller A, Hoornaert MT, Vandenbroeck S, Hermans J, et al. 192Ir Brachytherapy sources in Belgian hospitals. *Nucl Instrum Methods Phys Res A*. (1992) 312(1):251–6. doi: 10.1016/0168-9002(92)90164-Y
- 159. Dityuk A, Konobeyev AY, Lunev V, Shubin YN. New version of the advanced computer code ALICE-IPPE. (1998).
- 160. Szelecsényi F, Vermeulen C, Steyn GF, Kovács Z, Aardaneh K, van der Walt TN. Excitation functions of 186,187,188,189,190,192Ir formed in proton-induced reactions on highly enriched 192Os up to 66 MeV. *Nucl Instrum Methods Phys Res B.* (2010) 268(20):3306–14. doi: 10.1016/j.nimb.2010.07.010
- 161. Alam P, Laskar IR, Climent C, Casanova D, Alemany P, Karanam M, et al. Microwave-assisted facile and expeditive syntheses of phosphorescent cyclometallated iridium (III) complexes. *Polyhedron.* (2013) 53:286–94. doi: 10. 1016/j.poly.2013.01.045
- 162. Bura T, Retailleau P, Indelli MT, Ziessel R. Synthesis and properties of phosphorescent iridium (III) complexes of delocalized ligands. *Dalton Trans*. (2013) 42(13):4544–51. doi: 10.1039/c2dt32538a
- 163. Wu Q, Wang C, Song X, Zhang G. Microwave assisted synthesis of a new triplet iridium (III) pyrazine complex. *Chin J Chem Phys.* (2010) 23(3):355. doi: 10. 1088/1674-0068/23/03/355-357
- 164. Tárkányi F, Hermanne A, Takács S, Hilgers K, Kovalev SF, Ignatyuk AV, et al. Study of the 192Os(d,2n) reaction for production of the therapeutic radionuclide 192Ir in no-carrier added form. *Appl Radiat Isot.* (2007) 65(11):1215–20. doi: 10.1016/j.apradiso.2007.06.007
- 165. Dovbnya AN, Rogov YV, Shevchenko VA, Shramenko BI, Tenishev AE, Torgovkin AV, et al. A study of 192Ir production conditions at an electron accelerator. *Phys Particles Nuclei Lett.* (2014) 11(5):691–4. doi: 10.1134/S1547477114050112

- 166. Salvat F, Fernández-Varea J, Sempau J. PENELOPE—A Code System for Monte Carlo Simulation of Electron and Photon Transport. Paris: OECD Nuclear Energy Agency. (2011). p. 1–253.
- 167. Jayakody M, Jeyasugiththan J, Rajasooriyar C, Chougule A. Dosimetry procedure to verify dose in high dose rate (HDR) brachytherapy treatment of cancer patients: a systematic review. *Phys Med.* (2022) 96:70–80. doi: 10.1016/j.ejmp.2022.02.022
- 168. Roussakis Y, Anagnostopoulos G. Physical and dosimetric aspects of the iridium-knife. Front Oncol. (2021) 11:1–9. doi: 10.3389/fonc.2021.728452
- 169. Nohara T, Mizokami A, Kumano T, Shigehara K, Konaka H, Yoshifumi K, et al. Clinical results of iridium-192 high dose rate brachytherapy with external beam radiotherapy. *Jpn J Clin Oncol.* (2010) 40(7):677–83. doi: 10.1093/jjco/hyq016
- 170. Shigehara K, Mizokami A, Komatsu K, Koshida K, Namiki M. Four year clinical statistics of iridium-192 high dose rate brachytherapy. *Int J Urol.* (2006) 13(2):116–21. doi: 10.1111/j.1442-2042.2006.01243.x
- 171. Chin Y, Bullard J, Bryant L, Bownes P, Ostler P, Hoskin P. High dose rate iridium-192 brachytherapy as a component of radical radiotherapy for the treatment of localised prostate cancer. *Clin Oncol.* (2006) 18(6):474–9. doi: 10. 1016/j.clon.2006.04.005
- 172. Pötter R, Knocke T, Fellner C, Baldass M, Reinthaller A, Kucera H. Definitive radiotherapy based on HDR brachytherapy with iridium 192 in uterine cervix carcinoma: report on the Vienna university hospital findings (1993–1997) compared to the preceding period in the context of ICRU 38 recommendations. Cancer/Radiothérapie. (2000) 4(2):159–72. doi: 10.1016/S1278-3218(00)88900-3
- 173. Ott OJ, Pötter R, Hammer J, Hildebrandt G, Lotter M, Resch A, et al. Accelerated partial breast irradiation with iridium-192 multicatheter PDR/HDR brachytherapy. Strahlenther Onkol. (2004) 180(10):642. doi: 10.1007/s00066-004-1294-2
- 174. Abtahi M, Gholami S, Jassim H. High dose rate 192Ir versus high dose rate 60Co brachytherapy: an overview of systematic reviews of clinical responses of gynecological cancers from 1984 to 2020. *Biomed Phys Eng Express.* (2021) 7(5):055022. doi: 10.1088/2057-1976/ac1c52
- 175. Wen A, Wang X, Wang B, Yan C, Luo J, Wang P, et al. Comparative analysis of 60co and 192ir sources in high dose rate brachytherapy for cervical cancer. *Cancers (Basel)*. (2022) 14(19):4749. doi: 10.3390/cancers14194749
- 176. Strohmaier S, Zwierzchowski G. Comparison of 60 co and 192 ir sources in HDR brachytherapy. *J Contemp Brachytherapy*. (2011) 3(4):199–208. doi: 10.5114/jcb.2011.26471
- 177. Tantivatana T, Rongsriyam K. Treatment outcomes of high-dose-rate intracavitary brachytherapy for cervical cancer: a comparison of ir-192 versus co-60 sources. *J Gynecol Oncol.* (2018) 29(5):e86. doi: 10.3802/jgo.2018.29.e86
- 178. Bartoś B, Kowalska E, Bilewicz A, Skarnemark G. 103Ru/103mRh Generator. J $Radioanal\ Nucl\ Chem.\ (2009)\ 279(2):655-7.\ doi: 10.1007/s10967-008-7346-9$
- 179. Epperson CE, Landolt RR, Kessler WV. Solvent-solvent extraction of rhodium-103 m from ruthenium-103 employing a sulfate-carbon tetrachloride medium. *Anal Chem.* (1976) 48(7):979–81. doi: 10.1021/ac60371a031
- 180. Théry M, Alliot C, Huclier-Markai S. Recent progress in ruthenium chemistry for establishing a 103Ru/103mRh generator for auger therapy. *J Radioanal Nucl Chem.* (2024) 333(6):2723–33. doi: 10.1007/s10967-024-09484-9
- 181. Ohya T, Ichinose J, Nagatsu K, Sugo Y, Ishioka N, Watabe H, et al. Production of auger-electron-emitting 103mRh via a 103Pd/103mRh generator using an anion-exchange resin. *Radiochim Acta*. (2024) 112(1):37–43. doi: 10.1515/ract-2023-0238
- 182. Berk H. Development and evaluation of a 103Pd-/sup 103m/Rh radionuclide generator. Purdue Univ. (1971). p. 1–107. Available online at: https://www.proquest.com/docview/302539977?sourcetype=Dissertations%20&%20Theses (Accessed Accessed June 15, 2025).
- 183. Mamadaliev N, Levin V, Malinin A. Rhodium-103 m generator. *Radiokhimiya*; (USSR). (1978) 20(5):772–5.
- 184. Zagryadsky V, Korolev K, Kravets YM, Kuznetsova T, Kurochkin A, Makoveeva K, et al. Measurement of the rates of the pd () pd and ru () ru reactions in the horizontal channel of the IR-8 reactor at the NRC kurchatov institute. *Phys At Nucl.* (2024) 87(5):571–4. doi: 10.1134/S1063778824700571
- 185. Bernhardt P, Ahlman H, Forssell-Aronsson E. Model of metastatic growth valuable for radionuclide therapy. *Med Phys.* (2003) 30(12):3227–32. doi: 10.1118/1.1628851
- 186. Feng Y, Phelps TE, Carroll V, Gallazzi F, Sieckman G, Hoffman TJ, et al. Chemistry and radiochemistry of as, Re and rh isotopes relevant to radiopharmaceutical applications: high specific activity radionuclides for imaging and treatment. *Dalton Trans*. (2017) 46(42):14677–90. doi: 10.1039/C7DT02407J
- 187. Jurisson SS, Ketring AR, Volkert WA. Rhodium-105 complexes as potential radiotherapeutic agents. *Transition Met Chem.* (1997) 22(3):315–7. doi: 10.1023/A:1018441230403
- 188. Unni R, Mra P. Production and radiochemical separation of rhodium-105 for radiopharmaceutical applications. *Radiochim Acta.* (2002) 90:363–9. doi: 10.1524/ract.2002.90.6.363
- 189. Grazman B, Troutner D. 105Rh As a potential radiotherapeutic agent. Int J Radiat Appl Instrum A. (1988) 39(3):257–60. doi: 10.1016/0883-2889(88)90181-5

- 190. Brooks RC, Carnochan P, Vollano JF, Powell NA, Zweit J, Sosabowski JK, et al. Metal complexes of bleomycin: evaluation of [rh-105]-bleomycin for use in targeted radiotherapy. *Nucl Med Biol.* (1999) 26(4):421–30. doi: 10.1016/S0969-8051(98) 00109-7
- 191. Jia W, Ma D, Volkert EW, Ketring AR, Ehrhardt GJ, Jurisson SS. Production of No-carrier-Added105 rh from neutron irradiated ruthenium target. *Platinum Met Rev.* (2000) 44(2):50–5. doi: 10.1595/003214000X4425055
- 192. Okoye NC, Phelps TE, Charles A, McCormick JB, Wycoff DE, Lydon JD, et al. Recovery, recycling and re-irradiation of enriched 104Ru metal targets for cost effective production of 105Rh. *Appl Radiat Isot.* (2021) 176:109847. doi: 10.1016/j. apradiso.2021.109847
- 193. Goswami N, Higginbotham C, Volkert W, Alberto R, Nef W, Jurisson S. Rhodium-105 tetrathioether complexes: radiochemistry and initial biological evaluation. *Nucl Med Biol.* (1999) 26(8):951–7. doi: 10.1016/S0969-8051(99)00070-0
- 194. Krajewski S, Bilewicz A. The stability of the 105 [rh (16S 4 diol) cl 2]+ radiopharmaceutical precursor in solutions containing human plasma thiols. J Radioanal Nucl Chem. (2010) 285:293–300. doi: 10.1007/s10967-010-0577-6
- 195. Inagaki M, Sekimoto S, Tanaka W, Tadokoro T, Ueno Y, Kani Y, et al. Production of 47Sc, 67Cu, 68 ga, 105Rh, 177Lu, and 188Re using electron linear accelerator. *J Radioanal Nucl Chem.* (2019) 322(3):1703–9. doi: 10.1007/s10967-019-06904-z
- 196. Sciuto R, Festa A, Rea S, Pasqualoni R, Bergomi S, Petrilli G, et al. Effects of low-dose cisplatin on 89Sr therapy for painful bone metastases from prostate cancer: a randomized clinical trial. *J Nucl Med.* (2002) 43(1):79–86.
- 197. Kazakov AG, Babenya JS, Ekatova TY, Khvorostinin EY, Belyshev SS, Kuznetsov AA, et al. Production of 105Rh using electron accelerators and a new method for its recovery from irradiated targets. *Radiochemistry*. (2024) 66(3):356–63. doi: 10.1134/S1066362224030093
- 198. Khandaker MU, Kim K, Kim G. Production parameters of the therapeutic 105 rh radionuclide using medium energy cyclotron. *Pramana*. (2012) 79:243–8. doi: 10. 1007/s12043-012-0309-2
- 199. Ando A, Ando I, Tonami N, Kinuya S, Okamoto N, Sugimoto M, et al. Production of 105Rh–EDTMP and its bone accumulation. *Appl Radiat Isot.* (2000) 52(2):211–5. doi: 10.1016/S0969-8043(99)00129-3
- 200. Sanada S, Ando A, Ando I, Hiraki T, Hisada K. A single-strip mini-paper chromatographic method for rapid purity-control of 99mTc-labeled radiopharmaceuticals. *Eur J Nucl Med.* (1986) 12(8):390–3. doi: 10.1007/BF00252196
- 201. Kruper WJ Jr, Pollock DK, Fordyce WA, Fazio MJ, Inbasekaran MN. Functionalized polyamine chelants and radioactive rhodium complexes thereof for conjugation to antibodies. Google Patents (1991).
- 202. Pillai M, John C, Troutner DE. Labeling of human IgG with rhodium-105 using a new pentadentate bifunctional ligand. *Bioconjugate Chem.* (1990) 1(3):191–7. doi: 10.1021/bc00003a003
- 203. Pillai MRA, Lo JM, John CS, Troutner DE. Labeling of proteins using [105Rh] rh-4-(p-aminobenzyl)-diethylenetriamine. Int J Radiat Appl Instrum B. (1990) 17(4):419-26. doi: 10.1016/0883-2897(90)90111-D
- 204. Efe GE, Pillai M, Schlemper E, Troutner D. Rhodium complexes of two bidentate secondary amine oxime ligands and application to the labelling of proteins. *Polyhedron.* (1991) 10(14):1617–24. doi: 10.1016/S0277-5387(00)83772-9
- 205. Venkatesh M, Schlempe E, Jurisson S, Ketring A, Volkert W, Corlija M. Preparation of 105Rh labeled monoclonal antibody (MAb B72. 3) using aminobenzylpropyleneamineoxime as the bifunctional chelating agent; comparison to 131I labeled MAb B72. 3. *Radiochim Acta*. (1999) 85(3-4):157–64. doi: 10.1524/ract.1999.85.34.157
- 206. Pillai M, Lo J, Troutner D. Labeling of hematoporphyrin with 105Rh and binding studies with human gamma globulin. Int J Radiat Appl Instrum A. (1990) 41(1):69-73. doi: 10.1016/0883-2889(90)90132-Z
- 207. Venkatesh M, Goswami N, Volkert W, Schlemper E, Ketring A, Barnes C, et al. An rh-105 complex of tetrathiacyclohexadecane diol with potential for formulating bifunctional chelates. *Nucl Med Biol.* (1996) 23(1):33–40. doi: 10.1016/0969-8051 (95)02012-8
- 208. Li N, Eberlein C, Volkert W, Ochrymowycz L, Barnes C, Ketring A. Comparisons of 105Rh (III) chloride complexation with [14] aneNS3,[14] aneN2S2 and [14] aneN4 macrocycles in aqueous solution. *Radiochim Acta.* (1996) 75(2):83–96. doi: 10.1524/ract.1996.75.2.83
- 209. Li N, Struttman M, Higginbotham C, Grall A, Skerlj J, Vollano J, et al. Biodistribution of model 105Rh-labeled tetradentate thiamacrocycles in rats. *Nucl Med Biol.* (1997) 24(1):85–92. doi: 10.1016/S0969-8051(96)00177-1
- 210. Goswami N, Alberto R, Barnes CL, Jurisson S. Rhodium (III) complexes with acyclic tetrathioether ligands. Effects of backbone chain length on the conformation of the rh (III) complex. *Inorg Chem.* (1996) 35(26):7546–55. doi: 10.1021/ic960952z
- 211. Akgun Z, Engelbrecht H, Fan K-H, Barnes CL, Cutler CS, Jurisson SS, et al. The complexation of rhodium (III) with acyclic diaminedithioether (DADTE) ligands. *Dalton Trans*. (2010) 39(42):10169–78. doi: 10.1039/c0dt00813c
- 212. Smith C, Higginbotham C, Katti K, Volkert W. Rhodium-105 complexes of polydentate, aqueous-soluble, phosphine ligands: new radiochemical developments

- towards radioimmunotherapy. Phosphorus, Sulfur Silicon Relat Elem. (1999) $144(1):481-4.\ {\rm doi:}\ 10.1080/10426509908546286$
- 213. Cagnolini A, Ballard B, Engelbrecht HP, Rold TL, Barnes C, Cutler C, et al. Tetradentate bis-phosphine ligands (P2N2 and P2S2) and their rh(III), Ni(II) and 105Rh complexes: x-ray crystal structures of trans-[RhCl2(L2)]PF6, [Ni(L2)](PF6)2 and $\mu\text{-}O2SO2\text{-}[Ni(L5)]2(PF6)2$. Nucl Med Biol. (2011) 38(1):63–76. doi: 10.1016/j. nucmedbio.2010.06.013
- 214. Lommatzsch PK, Werschnik C, Schuster E. Long-term follow-up of ru-106/rh-106 brachytherapy for posterior uveal melanoma. *Graefe's Arch Clin Exp Ophthalmol.* (2000) 238(2):129–37. doi: 10.1007/PL00007880
- 215. Bergman L, Nilsson B, Lundell G, Lundell M, Seregard S. Ruthenium brachytherapy for uveal melanoma, 1979–2003: survival and functional outcomes in the Swedish population. *Ophthalmology.* (2005) 112(5):834–40. doi: 10.1016/j. ophtha.2004.11.038
- 216. Damato B, Patel I, Campbell IR, Mayles HM, Errington RD. Local tumor control after 106Ru brachytherapy of choroidal melanoma. *Int J Radiat Oncol Biol Phys.* (2005) 63(2):385–91. doi: 10.1016/j.ijrobp.2005.02.017
- 217. Schueler AO, Flühs D, Anastassiou G, Jurklies C, Neuhäuser M, Schilling H, et al. Beta-ray brachytherapy with 106Ru plaques for retinoblastoma. Int J Radiat Oncol Biol Phys. (2006) 65(4):1212–21. doi: 10.1016/j.ijrobp.2006.02.002
- 218. Abouzeid H, Moeckli R, Gaillard M-C, Beck-Popovic M, Pica A, Zografos L, et al. 106Ruthenium Brachytherapy for retinoblastoma. *Int J Radiat Oncol Biol Phys.* (2008) 71(3):821–8. doi: 10.1016/j.ijrobp.2007.11.004
- 219. Russo A, Laguardia M, Damato B. Eccentric ruthenium plaque radiotherapy of posterior choroidal melanoma. *Graefe's Arch Clin Exp Ophthalmol.* (2012) 250(10):1533–40. doi: 10.1007/s00417-012-1962-3
- 220. Belaïd A, Nasr C, Jmour O, Cherif A, Kochbati L, Bouguila H, et al. Brachytherapy of uveal melanomas with ruthenium-106 plaques. *Asian Pac J Cancer Prev.* (2016) 17(12):5281–5. doi: 10.22034/APJCP.2016.17.12.5281
- 221. Ghassemi F, Sheibani S, Arjmand M, Poorbaygi H, Kouhestani E, Sabour S, et al. Comparison of iodide-125 and ruthenium-106 brachytherapy in the treatment of choroidal melanomas. *Clin Ophthalmol.* (2020) 14:339–46. doi: 10. 2147/OPTH.\$235265
- 222. Takiar V, Voong KR, Gombos DS, Mourtada F, Rechner LA, Lawyer AA, et al. A choice of radionuclide: comparative outcomes and toxicity of ruthenium-106 and iodine-125 in the definitive treatment of uveal melanoma. *Pract Radiat Oncol.* (2015) 5(3):e169–e76. doi: 10.1016/j.prro.2014.09.005
- 223. Fili M, Astrahan M, Stålhammar G. Long-term outcomes after enucleation or plaque brachytherapy of choroidal melanomas touching the optic disc. *Brachytherapy.* (2021) 20(6):1245–56. doi: 10.1016/j.brachy.2021.05.162
- 224. Stålhammar G. Brachytherapy with 15- versus 20-mm ruthenium 106 plaques without verification of plaque position is associated with local tumor recurrence and death in posterior uveal melanoma. *Int J Radiat Oncol Biol Phys.* (2023) 117(5):1125–37. doi: 10.1016/j.ijrobp.2023.06.077
- 225. Mirshahi R, Sedaghat A, Jaberi R, Azma Z, Mazloumi M, Naseripour M. Ruthenium-106 plaque radiotherapy for uveal melanoma: analysis of tumor dimension and location on anatomical and functional results. *BMC Ophthalmol.* (2022) 22(1):309. doi: 10.1186/s12886-022-02521-9
- 226. O'Day RFJ, Roelofs KA, Negretti GS, Hay G, Arora AK, Stoker I, et al. Long-term visual outcomes after ruthenium plaque brachytherapy for posterior choroidal melanoma. *Eye.* (2023) 37(5):959–65. doi: 10.1038/s41433-022-01944-4
- 227. Grajewski L, Kneifel C, Wösle M, Ciernik IF, Krause L. Ruthenium-106 brachytherapy and central uveal melanoma. *Int Ophthalmol.* (2025) 45(1):23. doi: 10.1007/s10792-024-03381-6
- 228. Zuba I, Zuba M, Piotrowski M, Pawlukojć A. Ruthenium as an important element in nuclear energy and cancer treatment. *Appl Radiat Isot.* (2020) 162:109176. doi: 10.1016/j.apradiso.2020.109176
- 229. Zaitseva NG, Rurarz E, Vobecky M, Hwan K, Nowak K, Thétal T, et al. Excitation function and yield for 97Ru production in 99Tc(p,3n)97Ru reaction in 20–100 MeV proton energy range. *Radiochim Acta*. (1992) 56(2):59–68. doi: 10. 1524/ract.1992.56.2.59
- 230. Zaitseva NG, Stegailov VI, Khalkin VA, Shakun NG, Shishlyannikov PT, Bukov KG. Metal technetium target and target chemistry for the production of 97Ru via the 99Tc(p,3n) 97Ru reaction. *Appl Radiat Isot.* (1996) 47(2):145–51. doi: 10.1016/0969-8043(95)00272-3
- 231. Ditrói F, Hermanne A, Tárkányi F, Takács S, Ignatyuk AV. Investigation of the α -particle induced nuclear reactions on natural molybdenum. *Nucl Instrum Methods Phys Res B*. (2012) 285:125–41. doi: 10.1016/j.nimb.2012.05.030
- 232. Tárkányi F, Hermanne A, Ditrói F, Takács S, Ignatyuk A. Investigation of activation cross section data of alpha particle induced nuclear reaction on molybdenum up to 40MeV: review of production routes of medically relevant 97,103Ru. *Nucl Instrum Methods Phys Res B.* (2017) 399:83–100. doi: 10.1016/j.nimb.2017.03.043
- 233. Levkovskij V. Activation cross section nuclides of average masses (A=40-100) by protons and alpha-particles with average energies (E=10-50~MeV). Moscow, Russia (1991).

- 234. Graf HP, Münzel H. Excitation functions for α -particle reactions with molybdenum isotopes. *J Inorgan Nucl Chem.* (1974) 36(12):3647–57. doi: 10.1016/0022-1902(74)80143-0
- 235. Rapp W, Dillmann I, Käppeler F, Giesen U, Klein H, Rauscher T, et al. Cross section measurements of α -induced reactions on mo 92, 94 and sn 112 for p-process studies. *Phys Rev C Nucl Phys.* (2008) 78(2):025804. doi: 10.1103/PhysRevC.78.025804
- 236. Abe K, Iizuka A, Hasegawa A, Morozumi S. Induced radioactivity of component materials by 16-MeV protons and 30-MeV alpha particles. *J Nucl Mater.* (1984) 123(1):972–6. doi: 10.1016/0022-3115(84)90203-4
- 237. Sitarz M, Nigron E, Guertin A, Haddad F, Matulewicz T. New cross-sections for natMo(α ,x) reactions and medical 97Ru production estimations with radionuclide yield calculator. *Instruments*. (2019) 3(1):7. doi: 10.3390/instruments3010007
- 238. Happl B, Balber T, Heffeter P, Denk C, Welch JM, Köster U, et al. Synthesis and preclinical evaluation of BOLD-100 radiolabeled with ruthenium-97 and ruthenium-103. *Dalton Trans.* (2024) 53(13):6031–40. doi: 10.1039/D4DT00118D
- 239. Maiti M, Lahiri S. Measurement of yield of residues produced in 12C+ natY reaction and subsequent separation of 97Ru from Y target using cation exchange resin. *Radiochim Acta.* (2015) 103(1):7–13. doi: 10.1515/ract-2014-2277
- 240. Oster Z, Som P, Gil M, Fairchild R, Goldman A, Schachner E, et al. Ruthenium-97 DTPA: a new radiopharmaceutical for cisternography. *J Nucl Med.* (1981) 22(3):269–73.
- 241. Som P, Oster Z, Matsui K, Guglielmi G, Persson B, Pellettieri M, et al. 97 Rutransferrin uptake in tumor and abscess. *Eur J Nucl Med.* (1983) 8:491–4. doi: 10.1007/BF00598908
- 242. Borisova NE, Orlova MA, Knizhnikov VA, Dolgova VK, Reshetova MD, Orlov AP. First 97Ru complex with pyridine-2, 6-dicarboxamide conjugate for potential use as radiopharmaceutical. *Mendeleev Commun.* (2021) 31(2):207–9. doi: 10.1016/j.mencom.2021.03.020
- 243. Happl B, Brandt M, Balber T, Benčurová K, Talip Z, Voegele A, et al. Synthesis and preclinical evaluation of radiolabeled [103Ru]BOLD-100. *Pharmaceutics*. (2023) 15(11):2626. doi: 10.3390/pharmaceutics15112626
- 244. Esterlund RA, Pate BD. Analysis of excitation functions via the compound statistical model: angular momentum effects. *Nucl Phys.* (1965) 69(2):401–22. doi: 10.1016/0029-5582(65)90059-3
- 245. Mastren T, Radchenko V, Hopkins PD, Engle JW, Weidner JW, Copping R, et al. Separation of 103Ru from a proton irradiated thorium matrix: a potential source of auger therapy radionuclide 103mRh. *PLoS One.* (2017) 12(12):e0190308. doi: 10.1371/journal.pone.0190308
- 246. Blicharska M, Bartoś B, Krajewski S, Bilewicz A. Separation of fission produced (106)Ru from simulated high level nuclear wastes for production of brachytherapy sources. *J Radioanal Nucl Chem.* (2013) 298(3):1713–6. doi: 10.1007/s10967-013-2570-3
- 247. Tanabe M. Clinical trials on tumor scanning with 103Ru. $\it Radioisotopes.$ (1976) 25(232):10.3769. doi: 10.3769/radioisotopes.25.4_232
- 248. Wenzel M, Meinhold H, Schachschneider G. Ru-labeled ruthenocenoylglycine: comparison of clearance with hippuran. Eur J Nucl Med. (1985) 10:138–42. doi: 10.1007/BF00252722

- 249. Weiss A, Berndsen RH, Dubois M, Müller C, Schibli R, Griffioen AW, et al. In vivo anti-tumor activity of the organometallic ruthenium (II)-arene complex [ru (η 6-p-cymene) cl 2 (pta)](RAPTA-C) in human ovarian and colorectal carcinomas. Chem Sci. (2014) 5(12):4742–8. doi: 10.1039/C4SC01255K
- 250. Vojkovsky T, Sill K, Carie A. Manufacture of trans-[Tetrachlorobis (1h-indazole) ruthenate (iii)] and Compositions Thereof. Google Patents (2020).
- 251. Dash A, Chakravarty R. Radionuclide generators: the prospect of availing PET radiotracers to meet current clinical needs and future research demands. *Am J Nucl Med Mol Imaging*. (2019) 9(1):30–66.
- 252. Smith SV, McCutchan E, Gürdal G, Lister C, Muench L, Nino M, et al. Production of platinum radioisotopes at brookhaven linac isotope producer (BLIP). *EPJ Web Conf.* (2017) 146:09029. doi: 10.1051/epjconf/201714609029
- 253. Neves M, Kling A, Oliveira A. Radionuclides used for therapy and suggestion for new candidates. J Radioanal Nucl Chem. (2005) 266(3):377–84. doi: 10.1007/s10967-005-0920-5
- 254. Wren MS, May I, Guardincerri E, Boswell MS, Herman SM, Warzecha EJ, et al. Chemical separation and measurement of platinum activation products. *Talanta*. (2023) 260:124587. doi: 10.1016/j.talanta.2023.124587
- 255. Frindel M, Camus N, Rauscher A, Bourgeois M, Alliot C, Barré L, et al. Radiolabeling of HTE1PA: a new monopicolinate cyclam derivative for cu-64 phenotypic imaging. *in vitro* and *in vivo* stability studies in mice. *Nucl Med Biol.* (2014) 41:e49–57. doi: 10.1016/j.nucmedbio.2013.12.009
- 256. Lima LM, Esteban-Gomez D, Delgado R, Platas-Iglesias C, Tripier R. Monopicolinate cyclen and cyclam derivatives for stable copper (II) complexation. *Inorg Chem.* (2012) 51(12):6916–27. doi: 10.1021/ic300784v
- 257. Le Bihan T, Navarro A-S, Le Bris N, Le Saec P, Gouard S, Haddad F, et al. Synthesis of C-functionalized TE1PA and comparison with its analogues. An example of bioconjugation on 9E7. 4 mAb for multiple myeloma 64 cu-PET imaging. *Org Biomol Chem.* (2018) 16(23):4261–71. doi: 10.1039/C8OB00499D
- 258. Navarro A-S, Le Bihan T, Le Saëc P, Bris NL, Bailly C, Saï-Maurel C, et al. TE1PA As innovating chelator for 64Cu immuno-TEP imaging: a comparative *in vivo* study with DOTA/NOTA by conjugation on 9E7. 4 mAb in a syngeneic multiple myeloma model. *Bioconjugate Chem.* (2019) 30(9):2393–403. doi: 10.1021/acs.bioconjchem.9b00510
- 259. Ando A, Ando I, Tonami N, Kinuya S, Kazuma K, Kataiwa A, et al. 177Lu-EDTMP: a potential therapeutic bone agent. *Nucl Med Commun.* (1998) 19(6):587–92. doi: 10.1097/00006231-199806000-00012
- 260. Tinker ND, Zweit J, Sharma HL, Downey S, McAuliffe CA. Production of Nocarrier added 191Pt, a radiolabel for the synthesis and biological investigations of platinum anti-tumour compounds. *Radiochim Acta*. (1991) 54(1):29–34. doi: 10. 1524/ract.1991.54.1.29
- 261. Qaim SM, Hilgers K, Sudár S, Coenen HH. Excitation function of the 192Os (3He,4n)-reaction for production of 191Pt. *Appl Radiat Isot.* (2009) 67(6):1074–7. doi: 10.1016/j.apradiso.2008.11.008
- 262. Tárkányi F, Király B, Ditrói F, Takács S, Csikai J, Hermanne A, et al. Activation cross sections of proton induced nuclear reactions on iridium. *Nucl Instrum Methods Phys Res B.* (2005) 239(4):293–302. doi: 10.1016/j.nimb.2005.04.122
- 263. Tárkányi F, Király B, Ditrói F, Takács S, Csikai J, Hermanne A, et al. Cross sections of deuteron induced nuclear reactions on iridium. *Nucl Instrum Methods Phys Res B*. (2006) 247(2):210–6. doi: 10.1016/j.nimb.2006.03.002